Astrophysics and Space Science (2022) 367:121
https://doi.org/10.1007/s10509-022-04107-9

ORIGINAL ARTICLE

The *Polstar* high resolution spectropolarimetry MIDEX mission

Paul A. Scowen[1] · Ken Gayley[2] · Richard Ignace[3] · Coralie Neiner[4] · Gopal Vasudevan[5] · Robert Woodruff[6] · Roberto Casini[7] · Matt Shultz[8] · B.-G. Andersson[9] · John Wisniewski[10]

Received: 8 April 2022 / Accepted: 19 July 2022

Abstract

The *Polstar* mission will provide a space-borne 60 cm spectropolarimeter operating at ultraviolet (UV) wavelengths, capturing all four Stokes parameters (intensity, two linear polarization components, and circular polarization). *Polstar*'s capabilities are designed to meet its goal of determining how circumstellar gas flows alter and inform massive star evolution, affect the stellar remnant population, and stir and enrich the interstellar medium (ISM). These will be achieved by investigating the dynamical geometries in the winds and disks of hot stars, the composition and magnetic alignment of interstellar dust, and the star-forming accretion disks of UV-bright stars at an important transition boundary. Together these areas map out a kind of two-way interface between massive stars and their effect on our galaxy, wherein the stellar winds enrich the ISM with metals and kinetic energy, preconditioning their environment and the stellar endpoints prior to undergoing supernova. The ISM dust in turn reveals the composition and magnetic environment leading to new star formation, and the accretion disks of Herbig Ae/Be stars reveal how the ISM gas returns to make new massive stars. *Polstar* will combine high-resolution spectroscopy in the time domain with high-precision UV polarimetry. Doppler-shifted UV resonance line opacity will provide information about circumstellar kinematics, while polarization gives complementary geometric information about unseen structures. The composition and magnetic alignment of the smallest interstellar dust grains provides a probe of the ISM utilizing radiative alignment theory (RAT). *Polstar* will operate in the far-UV (FUV) at 122–200 nm at high spectral resolution of around $R \sim 30k$, and at FUV and near-UV (NUV) wavelengths of 122–320 nm at lower spectral resolutions of $0.1 - 1k$. Detection of polarization levels as weak as 0.1% are expected, with a temporal cadence ranging from 5–10 minutes for most wind variability studies, to hours or days for sampling rotation, to days or weeks for sampling binary orbits, to months to a year for sampling substructure in the inner regions of protoplanetary disks. Sub-meter-class aperture is well suited to access this wide array of time domain science, made possible by restricting to a few hundred bright, massive stars, necessarily extincted by a small to moderate column of interstellar dust, informing both the attributes of the stars and the ISM through which they are seen. As such, the focus is on our own galaxy and its evolutionary drivers, but a few targets in the Magellanic clouds offer the potential to extend this understanding to low-metallicity environments.

This article belongs to the Topical Collection: UV Spectropolarimetry for Stellar, Interstellar, and Exoplanetary Astrophysics with Polstar. Guest Editors: Paul A. Scowen, Carol E. Jones, René D. Oudmaijer.

✉ P.A. Scowen
paul.a.scowen@nasa.gov

1 NASA Goddard Space Flight Center, Greenbelt, MD 20771, USA

2 Department of Physics & Astronomy, University of Iowa, Iowa City, IA 52242-1479, USA

3 Department of Physics & Astronomy, East Tennessee State University, Johnson City, TN 37614-1700, USA

4 LESIA, Paris Observatory, PSL University, Sorbonne Université, Université Paris Cité, CNRS, 5 place Jules Janssen, 92195 Meudon, France

5 Lockheed Martin ATC, Palo Alto, CA 94034, USA

6 Woodruff Consulting, 2081 Evergreen Ave, Boulder, CO 80304, USA

7 High Altitude Observatory, NCAR, Boulder, CO 80301, USA

8 Department of Physics & Astronomy, University of Delaware, Newark, DE 19716, USA

9 SOFIA/USRA, NASA Ames Research Center, Moffett Field, CA 94035, USA

10 Department of Physics & Astronomy, The University of Oklahoma, Norman, OK 73019, USA

Published online: 14 December 2022

Keywords Polstar – NASA MIDEX · Far ultraviolet · Near ultraviolet astronomical observations · Extreme ultraviolet astronomy · Spectropolarimetry · Explorer · Massive stars · Interstellar medium · Exoplanet formation

1 Introduction

Understanding how a galaxy such as ours can evolve to support life requires understanding stellar feedback into star formation and the interstellar medium, and the processes that produce planets and promote their habitability. Though rare, massive stars are important because their impact is felt violently and immediately in the star-forming environment, whereas lower-mass stars provide a steadier and more global influence in the galaxy as a whole. The latter also incubate life by forming and maintaining planets. Our primary means of understanding these processes is by analyzing starlight that varies in intensity as a function of wavelength, angle (in the rare cases when spatial imaging is possible), polarization, and time.

A great deal of astronomical technology has already been aimed at the ultraviolet wavelength regime, but the domains of polarization and time variability remain largely unexplored. Though often at only a percent level or less, the degrees of polarization and time variability provide uniquely powerful constraints about the geometry and physical processes at play, as described further here. The purpose of *Polstar* is to access this unique information by combining high spectral resolution (resolution at the 10 km/s level) and high precision polarimetry (0.01% scale) with the ability to delve deeply into the time domain on a number of key benchmark targets.

This paucity of detailed constraints on geometry and dynamical variations is especially pronounced for massive stars, for which our extensive familiarity with the Sun is less relevant, and could therefore exhibit types of phenomena about which we remain as ignorant as we once were of Galileo's sunspots. Massive stars are generally distant point sources, so spatial resolution must be replaced by proxies such as frequency dependence induced by Doppler shifts in flows, and polarization induced by aspherical geometry. Also, the high luminosity of massive stars produce radiatively driven winds that remove so much mass it can alter their evolution and their impact on their galactic environment. In addition to steady winds, massive stars often partake in more impulsive events such binary mass transfer and eruptive incidents, which also alter their fates and their roles in a galaxy. Understanding the physics of these flows, and quantifying their impact, requires studying these variable behaviors on timescales from months to hours, and we cannot understand their physics, or properly constrain their mass fluxes, without understanding this behavior and its mysterious causes.

Polstar will approach these questions using dynamical spectra that are well resolved in wavelength and time, and augmented with polarimetric constraints, to probe wind structure and correct the mass-loss rate for the effects of wind clumping and asphericity. Processes that spin up and spin down these stars will also be studied from a geometric and time-dependent perspective, as angular momentum evolution affects the nature of the endpoints and supernova types, such as gamma-ray bursts and black hole binary mergers. The role of magnetism will be considered by measuring circular polarization from the Zeeman effect, where knowledge of the photospheric magnetic field and the modification of the circular polarization induced by the hypersonic acceleration of a wind uniquely constrains models of wind initiation and informs the causes and properties of massive star magnetism.

Ultraviolet (UV) spectropolarimetry will provide new constraints on the smallest dust grains in the interstellar medium (ISM), which play an important role in galactic chemistry, star formation, and the propagation of ionizing radiation. Pursuing this, we seek a better understanding of how the FUV and EUV align the smallest grains in a magnetic field, how different EUV environments can lead to a difference in the grain size at maximum alignment, how this depends on the metallicity in the chosen sightline, and what is the source of the mysterious 2175 Angstrom extinction feature.

These objectives involve how ISM dust and gas respond to magnetic fields and ionizing radiation. UV spectropolarimetry allows probes of the smallest dust, which has the most significant impact on the short wavelengths of ionizing radiation. This connects with radiative reprocessing, understanding cosmological backgrounds, and constraining the degree of ionization in the ISM. EUV radiation shortward of the Lyman limit plays an important role, is difficult to observe directly, and along with magnetic fields, contributes to regulating galactic plasma dynamics.

The final area of interest includes the processes that assemble and maintain exoplanets, and contribute to transient events that could challenge prolonged habitability. One type of transient event, atmospheric blowoff triggered by stellar activity, can be explored entirely spectroscopically, and requires a relatively low signal-to-noise of around 10 in order to correlate the appearance of absorption lines during ingress or egress of transiting planets with strong stellar flares in active dwarfs. Owing to the low signal level required to distinguish transient line events, blowoff events at 10 km/s resolution can be detected transiting the brightest active dwarfs in impulsive minute-long timescales.

The FUV spectroscopically provides access to an entire suite of resonant diagnostic lines that can map a large variety of physical phenomena from gas and plasma electron

densities and temperatures, to gas mass flows, stellar rotational speeds, plasma optical depths, and metallicities of material in the gas phase (Scowen et al. 2017). Measurements of these diagnostics can be done either in emission or in absorption depending on the physical nature of the system under scrutiny. These merits have been long understood and have made UV spectroscopy of great value to the astronomical community through missions and instruments such as *IUE* (Macchetto 1976), *HUT* (Davidsen and Fountain 1985), *EUVE* (Bowyer et al. 1981), *HST-STIS* (Gull et al. 1986), *FUSE* (Moos 1991), and *HST-COS* (Green et al. 1998).

The legacy of *Polstar* extends to earlier missions such as *WUPPE* (Nordsieck et al. 1994) and *HST-FOS* (Ford 1990) which provided pathfinding capabilities in polarimetry, but with recent advances in polarimetric techniques (Neiner 2015), UV coatings (Quijada et al. 2017) and UV solid state detectors (Nikzad et al. 2020), married with innovative optical design, we stand ready to deliver orders of magnitude improvement in performance over those earlier missions, some 25 years after they were in service. The time is ripe for a renaissance in FUV spectropolarimetry and this paper outlines both the science we seek to advance and the design features that will enable these advances, that takes advantage of the projected performance of the observatory.

We will "close the loop" of massive star impacts on the ISM by measuring UV extinction and polarization by grains < 0.3 μm, whose composition and magnetic alignment depend on chemical enrichment by massive-star evolution (Hoang and Lazarian 2016).

Mass flow in the inward direction across the interface with the ISM is responsible for the very existence of massive stars, and *Polstar* will investigate the complex geometry in the innermost regions of that process by exploring the delivery of mass from the accretion disk to the forming star. It will also map the transition from magneto-accretion to boundary layer accretion (Wichittanakom et al. 2020).

This paper is organized to describe more details about the objectives of *Polstar* science in §2, including the importance of UV spectropolarimetry in the time domain for understanding massive star winds, disks, and mass flows, and interstellar dust inputs, and certain UV-accessible aspects of protoplanetary disks. The instrumentation that will accomplish this, and its calibration, is detailed in §3, and a summary is given in §4.

2 The science of *Polstar*

The *Polstar* mission will provide sensitive measurements of 3D structures at the interfaces between massive stars and their environment. These structures regulate the evolution of the mass and angular momentum of massive stars, stars that originate from the ISM and largely return to it, enriching it with elements necessary for life.

2.1 The interface between stars and ISM

In order for the ISM to increase its chemical enrichment via stellar nucleosynthesis, it must maintain that enrichment against the steady escape induced by galactic outflows, and against dilution by infalling cosmologically pristine material (Péroux and Howk 2020). This competition is the "baryon cycle," and is regulated by the ISM as it forms stars, and by stars as they return mass and energy to the ISM.

Through spectropolarimetric observations in the time domain, *Polstar* is optimized to probe the complex structures necessary to understand this interface, which is neither smooth nor spherically symmetric (Hillier 2020). Understanding the complexities of how it operates is crucial, because observations (Mollá et al. 2015) show that metallicity in the solar neighborhood rose rapidly during the first 1-2 Gyr after formation of the Milky Way. Only the short life-cycle of massive stars can produce such a rapid rise.

On the inbound side of this interface is mass accretion where the inner and most UV-bright layers involve transient dynamics that support planet formation alongside star formation (Hartmann et al. 1998; Andrews 2020). On the outbound side are winds, disks, and binary mass transfer. These control the mass and angular momentum inputs that set the stage for supernovae (SNe) and kilonovae (KNe) progenitors that cannot be understood without tracking preceding stages (Smartt 2015), as these stages alter not only the exploding star, but also the environment into which that star explodes.

Within the ISM itself, the cumulative effects of this interface affect the composition and size distribution of dust formation, manifested in the UV via extinction and polarization induced by the smallest grains (< 0.3 μm). Along with chemical enrichment, massive stars add ionizing radiation (Schaerer and de Koter 1997; Kudritzki 2002), which along with interstellar magnetism, can lead to ground state alignment (GSA; Yan and Lazarian 2006, 2012) of metal ions in the ISM.

These features weave together the complex interaction zones between the ISM and the massive stars it produces, providing a rapid channel for feedback into the nature of the ISM. Understanding these aspects of galactic evolution is the ultimate science goal of *Polstar*.

2.2 The role of UV spectropolarimetry

The fundamental obstacle to understanding the star-ISM interface is the impossibility of seeing massive stars at the detail we see our Sun. This leaves unclear the basic processes and structures involved, so we must use proxies for

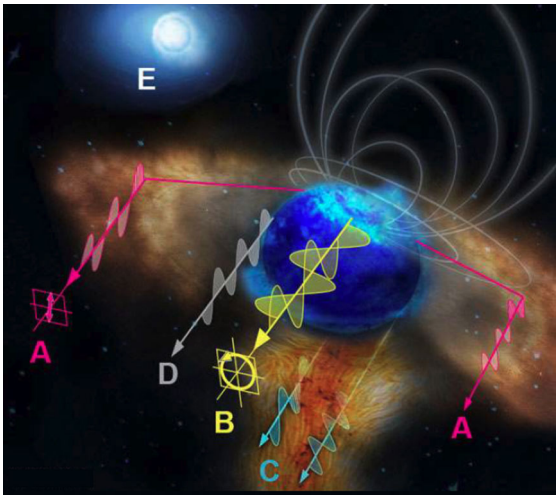

Fig. 1 Polarizing Scenarios. Schematic encapsulating polarigenic mechanisms to be addressed by *Polstar*: a massive star (center), circumstellar disk and scattered light (A), magnetism and the Zeeman effect (B), ISM polarization (C), limb polarization (D), and binarity (E). Scattered light at (A) is linearly polarized; light at B is circularly polarized; (C) represents both extinction and addition of linear polarization by grains; (D) identifies linearly polarized light from the stellar atmosphere; and (E) signifies a secondary illuminating source of scattered light from a binary companion

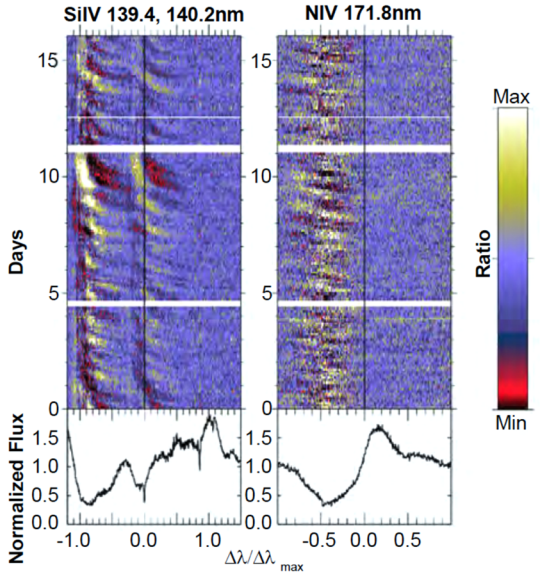

Fig. 2 *IUE* Dynamical Spectra. Structured outflows revealed in dynamical *IUE* spectra (colored) show deviations from time averaged UV P Cygni lines (bottom) for O supergiant zeta Pup (Massa and Prinja 2015). The abscissa is wavelength-shift from line center (normalized to maximal). Features are seen to propagate outward in the wind, but at SNR 20, only globally organized structures are revealed. The implications for mass-loss rates of small-scale clumping expected from theory (Hillier 2020) requires *Polstar*'s SNR∼ 300 (Gayley et al. 2022). Reproduced with permission

spatial information (Fig. 1). These include Doppler shifts of high-opacity UV resonance lines (c.f., the "P Cygni" profiles at bottom in Fig. 2), which allow velocity mapping along the line of sight. But this is most sensitive as a 1D probe of flow seen in projection against the face of the star. Compact structures that appear away from the face of the star can be more sensitively probed with linear polarization produced by dipole scattering. Hence the combination of spectroscopy and polarimetry provides more complete information to resolve geometric ambiguities (e.g., Harries and Howarth 1996; Harries et al. 2002; Ababakr et al. 2015; St-Louis et al. 2018).

For example, a smoothly varying difference in wind optical depth contrast between pole and equator induced by a preferred rotation axis produces a linear polarization that depends on both the viewing inclination and density contrast. The asphericity also alters the shape of the P Cygni line profile (Bjorkman et al. 1994), and combining these effects provides complementary information capable of separating inclination from density contrast (Petrenz and Puls 2000; Gayley et al. 2022).

Another example of the complementarity of spectral and polarimetric information is the fact that structures seen in projection against the stellar disk are readily detected by their spectroscopic absorption features, whereas structures seen well away from the star produce polarization by virtue of the scattering angle. *Polstar* capitalizes on this complementarity to probe the signatures of rotation, magnetism, and binary interaction, and how they affect massive star evolution, its impact on the ISM, and the final stages of accretion and planet-building.

The data to be returned includes all four Stokes parameters: total intensity (I), linear (Q and U) and circular (V) polarizations, as functions of wavelength. When also tracked in the time domain to reveal transient, rotating, and orbiting structures, *Polstar* offers a unique opportunity to understand the stellar-ISM interface.

2.3 The role of time series

Time series are critical for probing the dynamically varying attributes of rotating and orbiting stars and disks. Temporal modulation permits separation of intrinsic polarization from induced ISM polarization. Time series also expose stochastic structures, and allow asymmetrical structures to be seen from varying angles. The observing strategy will be to access a sufficiently large sample to represent relevant stellar classes, yet small enough to allow substantial time monitoring and phase coverage.

2.4 The massive star side of the stellar-ISM interface

The most massive stars contribute strongly to the ISM via radiatively driven winds that can have a billion times the mass flux of the solar wind (Lancaster et al. 2021). This mass loss

can alter the stellar evolution and change the initial conditions for later phases of evolution, including SNe (Langer 2012).

2.4.1 Structured winds

Hot-star mass-loss rates are often inferred from radio continuum and optical recombination lines, both of which are enhanced by wind clumping (Langer 2012; Gayley et al. 2022). Hence, these diagnostics require downward corrections (Nugis et al. 1998; Bouret et al. 2005; Muijres et al. 2011), since clumping is expected due to nonlinearities in the spectral line-driving of hypersonic winds (Sundqvist et al. 2018; Owocki et al. 1988). Current poorly constrained clumping prevents knowing true mass-loss rates within a factor of 2 or worse (Puls et al. 2008).

Polstar will address this pressing problem using continuous wind monitoring of the brightest target massive stars to track resolved structures at 400 s sampling as they accelerate (at ~ 0.03 km/s^2) through the local linewidth (~ 10 km/s). This will enormously improve the dynamical spectra seen in Fig. 2 (Massa and Prinja 2015) by providing SNR > 300, compared to ~ 20 for *IUE*, to quantify the impact of clumping on inferred mass-loss rates (Gayley et al. 2022).

Fig. 2 shows that when only the SiIV line is considered, the periodic large-scale signal visible in *IUE* data appears to initiate in the wind, but when the NIV line formed closer to the surface is included, features track right to the surface (Massa and Prinja 2015). With *Polstar*'s much higher SNR, this question can be answered for dense small-scale clumps using line ratios from doublets, such as SiIV 140 nm (Prinja and Massa 2010).

In addition to small-scale clumping, *Polstar* will also explore quasi-periodic Discrete Absorption Components (DACs; Kaper et al. 1997), apparent in Fig. 2. DACs are believed to be related to Co-rotating Interaction Regions (CIRs; Mullan 1984; Cranmer and Owocki 1996), but questions remain about their causes and impact on mass-loss rate determinations (Massa and Prinja 2015; Gayley et al. 2022). Simultaneous photometric variations at the ~ 2 mmag level can be tracked at several-minute timescales to connect wind and photospheric variations using *Polstar* (Gayley et al. 2022).

The spectroscopic information will be complemented with polarization. Simultaneous linear polarization co-added over ~ 200 km/s bins raises the ~ 300 SNR at 20 km/s resolution to the ~ 1000 level for 1×10^{-3} precision. This precision is adequate for detection of stochastic and rotationally modulated polarizations within lines and in the continuum for order-unity density contrasts in strong winds with free electron optical depth above about 0.1 (Ignace et al. 2015; Hillier 1996; Dessart and Hillier 2011). Polarization variations can then be connected with simultaneous spectroscopic signatures linked to clumping (Fox and Henrichs 1994; Brown et al. 1995; Richardson et al. 1996; Rodrigues and Magalhães 2000; Li et al. 2009; Davies et al. 2007; Gayley et al. 2022), to provide independent geometrical constraints on these ubiquitous features.

2.4.2 Magnetic stars

The strong (kG) magnetic fields found in some massive stars, $\sim 10\%$ of the monitored sample (Grunhut et al. 2017; Sikora et al. 2019), have a dramatic impact on circumstellar structure. Strong fields corral wind flows, reducing the net mass-loss rate by up to $10\times$ (ud-Doula and Owocki 2002), possibly enabling heavy black hole formation at high galactic metallicity (Petit et al. 2017). With rapid rotation, centrifugal support of co-rotating circumstellar material prevents infall (Townsend and Owocki 2005), building up density and angular momentum in a "centrifugal magnetosphere" until it breaks out, taking the angular momentum with it (Ud-Doula et al. 2008; Shultz et al. 2020). Even modest mass-loss can lead to rapid spindown, resulting in slow rotational periods up to 50 years long. Spindown lowers the centrifugal support, allowing the contained wind to fall inward via a "dynamical magnetosphere" (Ud-Doula et al. 2009; Shultz and Wade 2017; Shultz et al. 2019).

This paradigm is illustrated in Fig. 3, showing that magnetic inhibition increasingly reduces mass-loss as angular momentum is lost and centrifugal breakout weakens. The associated optical emission is also lost (Shultz et al. 2019), but UV resonance-line opacity continues to reveal the dynamical magnetosphere (Petit et al. 2013).

Combining spectroscopy and polarimetry, *Polstar* data can be used to generate 3D maps of the magnetic, velocity, and density structure (Shultz et al. 2021) as depicted schematically in Fig. 3, to test that the trapped wind is returned by fallback onto the star. Quantitative tests of this expectation involve spectroscopic evidence of infall from redshifted absorption (Erba et al. 2021a). Detection requires phase sampling over the rotation period to monitor the variable absorption with changing perspective, and when possible the polarization, to be seen in stereoscopic detail (Erba et al. 2021b), in keeping with the mission's emphasis on time-domain science.

For the strongest fields (~ 10 kG), *Polstar* allows magnetism in the wind to be detected for the first time via circular polarization induced by the Zeeman effect (c.f., Fig. 1(B), Donati and Landstreet (2009)). For detecting fields in the photosphere, the established technique of least-squares deconvolution (LSD) (Donati et al. 1997; Kochukhov et al. 2010; Wade et al. 2000; Ud-Doula et al. 2009; Shultz et al. 2022) has shown that coadding a large number of optical absorption lines at a level of polarization precision of 2×10^{-4} is sufficient to detect and track modulations in the circular polarization (Stokes V) profiles. *Polstar* will extend and augment this capability into the UV by

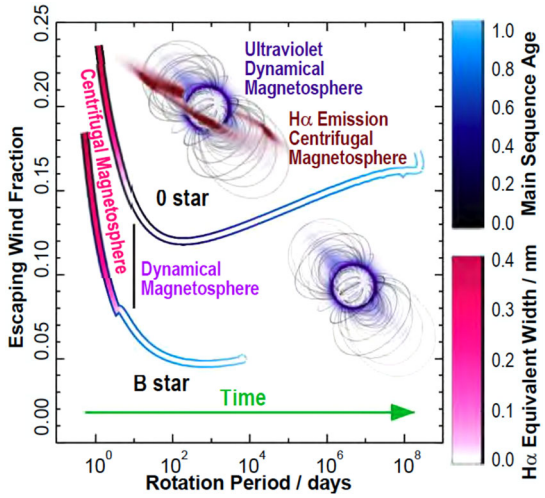

Fig. 3 Magnetospheres in the UV. Magnetospheres can limit the mass-loss escaping the wind (Ud-Doula et al. 2008), here shown against rotation period (proxy for time via magnetic braking). O and B star tracks are plotted (Keszthelyi et al. 2020). Insets suggest when Hα is observable, but higher opacity UV resonance lines detectable by *Polstar* produce observable diagnostics at every stage (Oksala et al. 2015; Owocki et al. 2016), including absorption against the face of the star, and scattering and polarization in the extended environment

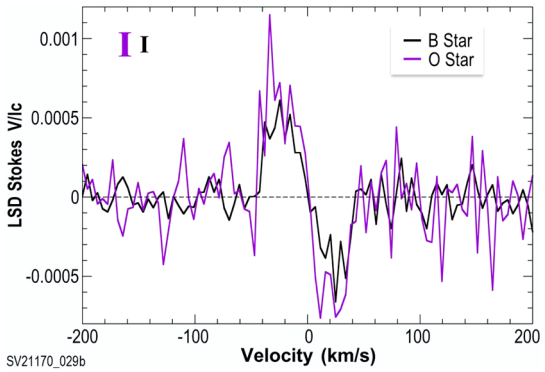

Fig. 4 UV Magnetometry. Modeled Stokes-V profiles from the LSD method for O and B stars with surface field of 3 kG for SNR=100 per resel, requiring resolution R=30k and LSD-improved polarization precision 2×10^{-4}. Representative errors indicated at upper left

taking advantage of the increased photon flux and the more numerous and stronger lines present there (Fig. 4), allowing LSD to detect kG-level surface fields at a necessary SNR level of only / 100 per resolution element (Folsom et al. 2022), which effectively offsets the inherent disadvantages of using space-based UV.

Also, for the first time, we expect to detect the Hanle effect in UV resonance scattering lines in massive stars (Folsom et al. 2022), a diagnostic successfully used in solar studies (e.g., Stenflo 1982; Ishikawa et al. 2017). The Hanle effect is sensitive to 1-100 G magnetic fields (Stenflo 1994). Operating in linear polarization, studies of photospheric lines (c.f., Fig. 1(D)) can detect generally weaker fields than with the Zeeman effect (Manso Sainz and Martínez González 2012), and with circumstellar lines (c.f., Fig. 1(A)), magnetism in winds and magnetospheres is detectable (Ignace et al. 2004).

2.4.3 Interacting binaries

The majority of massive stars will undergo binary mass transfer in their lifetime (Sana et al. 2013), which can most prominently affect the stellar spin via transfer of orbital angular momentum. When this transfer is non-conservative, it can also significantly affect the total mass and orbital angular momentum of the system. Both these effects have ramifications for galactic evolution through the massive star final states and their KNe, SNe, and gamma-ray bursts, and are relevant for heavy black holes as sources of gravitational wave events (de Mink et al. 2013). *Polstar* will provide unique insights into these processes with its signature combination of measuring absorption in UV resonance lines and polarization from free-electron scattering (Jones et al. 2022; Peters et al. 2022).

Stellar evolution models for single stars predict rotation evolution for a range of initial rotation rates (Eggenberger et al. 2008; Brott et al. 2011; Georgy et al. 2013). Wind angular momentum loss (even in non-magnetic stars) may spin a star down faster than evolutionary pressures can spin it up, while binary interactions can boost the spin rate (Kerber et al. 2004). *Polstar* will test whether binary mass transfer plays an essential role in stellar spinup, by surveying ~ 200 stars with evidence of near-critical rotation (such as the presence of a disk) for evidence of binarity. If a classical Be star is spun up by mass stripping from a companion, that companion will be present as a late-type subgiant (like CX Dra), a hot subdwarf (sdO), or compact object (Jones et al. 2022). The first and last are easily detected in the optical-IR and X-ray regions, but FUV spectra of high R and SNR are needed to detect sdO objects. Confirmation of an sdO companion to the bright Be star phi Per from *IUE* spectra (Thaller et al. 1995) suggests large numbers of stripped cores of previously more massive stars.

A hidden sdO (c.f., Fig. 1(E)) with low luminosity can be identified spectroscopically in the UV via its much narrower lines than the larger mass gainer (Jones et al. 2022). Fig. 5 shows that sdO companions with luminosities as low as 1×10^{-3} of the mass gainer can be detected using R=30k and SNR of 300, which provide the instrumental requirements to discover a host of sdO companions. Orbital solutions are obtainable for high-inclination systems through spectral variations.

Polstar can be used to determine how close the rotation of the mass gainer is to critical (Jones et al. 2022), to correlate high rotation with the presence of a companion. Net linear polarization from rotationally oblate stars (c.f., Fig. 1(A),

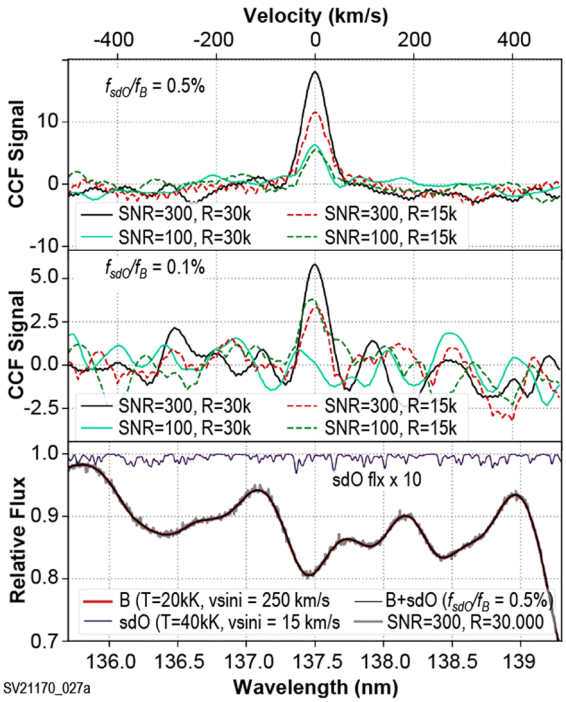

Fig. 5 Finding Stripped Companions. Cross-correlation function signals for different SNR and resolution. The relative flux contribution from the sdO component (fsdO/fB) is 0.5% (top) and 0.1% (mid), and centered at zero velocity. Bottom shows a portion of the composite spectrum for fsdO/fB = 0.5%, with isolated 10× sdO flux plotted above. The simulation incorporates the SNR and R values as indicated

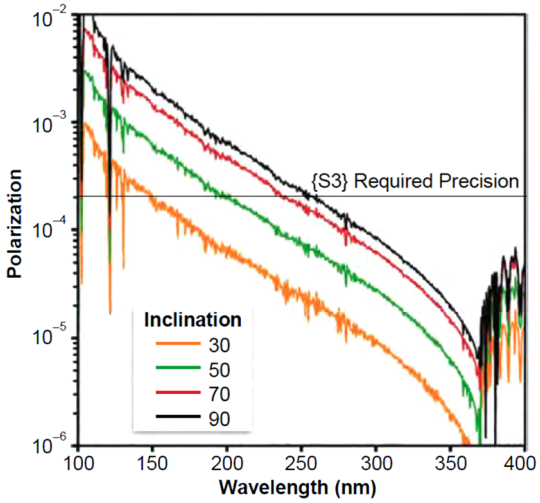

Fig. 6 Critical Rotation in the FUV. UV model polarization based on Regulus known to rotate at 96.5% critical for a range of viewing inclinations from (Cotton et al. 2017). The steeply rising polarization values in the FUV observable with Ch2 is typical of all near-critical rotating massive stars. The horizontal line shows the precision of 2×10^{-4} that will be achievable with the *Polstar* design

(Jones et al. 2022)) rises steeply into the FUV (Fig. 6), and this telltale signature is easily separable from disk and ISM polarization (c.f., Fig. 1(A&C), (Andersson et al. 2022)). Inclination can be separated from rotation by combining polarization with spectral linewidth (Jones et al. 2022).

To allow statistical tests of the ubiquity of previously unseen stripped companions, ~ 200 rapid rotators will be targeted. Given the effective area (Fig. 10), exposures < 1 hour provide the necessary SNR ~ 300 at R = 30 k (see Fig. 5).

The techniques involve searches for spectral features combined with continuum polarization from binaries in the throes of mass transfer, or shortly thereafter, with emphasis on close binaries with a subgiant member seen at high inclination to catch mass transfer in the act (Peters et al. 2022). A selective list (20+ targets) is used with known orbital characteristics. These will be visited ~ 20 times per orbit to map signatures of mass transfer streams (via UV resonance-line absorption in Ch1) and non-conservative polar outflows (via linear polarization in Ch2). For example, polar outflow and accretion disk are distinguished in polarization in wavelength dependent Position Angle (PA) changes, for beta Lyr at the 2×10^{-3} level (Hoffman et al. 1998). This constrains accretion and mass loss in the binary mass transfer.

2.4.4 Colliding winds

Polstar will observe orbitally-phased spectra and polarization from massive binaries, in which one star shines like a searchlight through its companion wind (c.f., Fig. 1(E), St.-Louis et al. 1993). This searchlight provides a powerful probe of wind kinematics, and will be used to test the possibility that multiline scattering in the radiative driving of denser winds yields more spatially extended wind acceleration (Sander et al. 2020) than does the freely escaping radiation in weaker winds.

Time-domain observations will also constrain the opening angle of the colliding-wind bow shock, a telling diagnostic because it depends on the wind momentum ratio (Eichler and Usov 1993), providing a unique and complementary constraint on the relative mass fluxes (Cantó et al. 1996; Gayley 2009). Also observationally accessible in colliding-wind systems will be enhanced UV continuum polarization, stemming from free-electron scattering of the companion starlight in the bow shock where the primary wind piles up (Harries et al. 2000; St-Louis et al. 2022). Orbital modulation of this feature distinguishes its polarization signal from interstellar, allowing independent constraints on wind structure that quantify the wind density and momentum flux at the location of the companion (St-Louis et al. 2022; Fullard 2020).

Polstar will observe 20 massive binaries with 10–20 selected phase samples per target of various types (WR+OB, OB+OB) to measure the radial acceleration of winds using systems of different wind densities and binary separations (St-Louis et al. 2022). The polarization from the colliding

wind shock cone will show chromatic effects at a level of $\sim 5 \times 10^{-4}$, requiring SNRs of 1000 s (Harries et al. 2000; St-Louis et al. 2022; Hillier 1996). Combined with variable line profile shapes caused by the wind eclipse at SNRs of 100 s will distinguish acceleration models (St-Louis et al. 2022).

2.5 The ISM side of the interface

The impact of massive stars on the ISM comes in many forms: chemical enrichment, ionizing radiation, cosmic ray heating from SNe, interstellar gas flows, and magnetic field generation (Beck et al. 1996). All these effects relate to dust grain composition and alignment (Andersson et al. 2015), accessible via ISM polarization (c.f., Fig. 1(C)). Hence separating this component from intrinsic stellar polarization provides a diagnostic of how massive star winds and SNe impact the galactic dynamo (e.g., Butsky et al. 2017), the distribution and chemistry of the grains, and the overall massive star/ISM interface.

2.5.1 ISM linear polarization

Interstellar polarization is due to dichroic extinction by dust grains with an elongated axis that is aligned (typically) perpendicular to the local magnetic field (Hiltner 1949). This occurs when silicate grains are spun up by radiative torques (Andersson et al. 2015). When anisotropically illuminated by wavelengths less than the grain radius, solidstate processes ((“The Barnett effect;” Purcell 1979) cause grain alignment both internally (along a grain symmetry axis) and externally (along an external reference line), and the paramagnetic grains that experience both alignments induce polarization. Carbon solids are diamagnetic and not normally responsive to alignment, so the convolution of grain sizes, mineralogy and illuminating Spectral Energy Density (SED) is encoded in the observed polarization curve.

This Radiative Alignment Torque (RAT) paradigm (Lazarian and Hoang 2007) provides a quantitative theory for inverting the polarization to extinction curve into grain properties, mineralogy, and environmental parameters including interstellar magnetism, radiation field Spectral Energy Density (SED) and the gas density (which randomizes grain orientation). The UV probes the smallest grains in this distribution, which significantly cool the gas and affect galaxy and star formation (Misselt et al. 2001).

2.5.2 Serkowski and super-Serkowski

The convolution of the total grain size distribution (a power-law; Mathis et al. (1977)), the SED, the alignment efficiency (RAT), and (Mie) scattering physics, leads to the “Serkowski function” shape of the dichroic extinction polarization curve

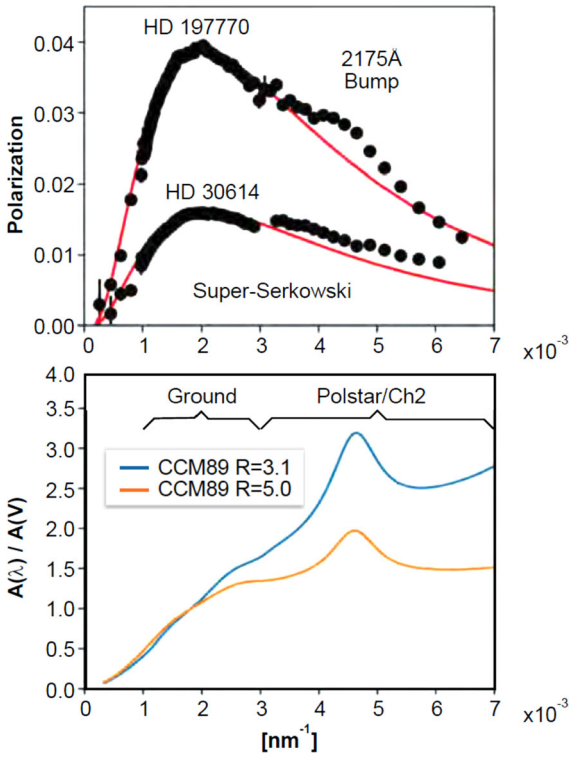

Fig. 7 The UV Perspective on ISM Grains. Previous UV polarimetry with *WUPPE* (note errors typically smaller than the points) has shown a number of poorly understood phenomena (Anderson et al. 1996). (top) For $\sim 30\%$ of the sightlines, the UV polarization exceeded that inferred from the NIR/Optical, known as the Super-Serkowski effect. For $\sim 5\%$ of the targets, polarization (top) was seen in the 2175 Å extinction feature (bottom). *Polstar* detects extinction and polarization to the right of 3×10^{-3} nm^{-1}. (CCM: Cardelli et al. (1989a); $R = R_V$, total to selective extinction)

from the UV to near-IR wavelengths (Fig. 7, e.g., Clayton et al. (2003)).

This curve is shaped by the relative abundance of silicate and carbon grains as a function of size (Draine and Fraisse 2009). Comparing the polarization from regions with varying metallicity reveals how the mineralogy for different grain sizes depends on the cosmo-chemistry (Hensley and Draine 2021). Comparing the relative and absolute polarization over wavelength (Fig. 7) with existing emission polarization (e.g., *Planck*) and tracers of the column density and environment, allows polarization efficiency to be inferred, relevant to alignment, turbulence, and magnetic field geometry (Panopoulou et al. 2019).

The relative size of the grains and the wavelengths of the illuminating radiation affects the alignment efficiency (Lazarian and Hoang 2007). In most of the ISM, light shortward of the Lyman limit cannot propagate and therefore limits the size of the smallest aligned grains. In regions fully ionized by hot stars, grains with diameters smaller than d=0.09 μm (=90 nm) can, under RAT theory, be aligned by the radiation

from nearby hot stars, enhancing the UV polarization curve at shorter wavelengths to provide a probe of the stellar EUV.

This so-called "Super-Serkowski polarization" was detected in 7 of the 28 stars observed by *WUPPE* (Fig. 7; Martin et al. (1999), Nordsieck et al. (1994)). All 7 sightlines probed the Per OB3 super-bubble, suggesting that enhanced UV polarization occurs when EUV irradiation internal to the super-bubble meets small grains at its fringes. Confirming and expanding the sample of this effect in Per OB3, and in other selected ionized regions, will probe the unseen EUV SED in such super-bubbles.

2.5.3 Spectral features; the 2175 Å bump

A spectral feature known as the 2175 Å (217.5 nm) extinction "bump" shows an associated polarization excess (see Fig. 7) but only in 2 of the 28 lines of sight currently probed. This small relative number may be related to the expectation (Whittet 2003) that the carrier of the feature is very small carbon particles. The two sightlines showing "bump polarization" are both toward regions of intense star formation, suggestive of processing allowing the small carbon dust grains in these environments to align. Determining the carrier of the 2175 Å feature, and testing explanations for its alignment, requires increasing the sample to well above 100.

This 2175 Å polarization excess might only be 2×10^{-3} (Wolff et al. 1997), seen against a broad polarization of some 10^{-2} (Fig. 7). Defining the FWHM of this feature in wavelength requires measuring 10^{-3} at a precision of 3×10^{-4}, which the *Polstar* design will supply.

2.5.4 Low metallicity environments

It is now clear that the standard Milky Way extinction curve based on a single parameter, the total-to-selective extinction value (R_V), cannot be applied to dust extinction in other galaxies. The canonical extinction curve derived by (CCM Cardelli et al. 1989b) was based on sightlines within 1 kpc of the Sun, and so only a very small volume of our own galaxy was mapped out. It is clear that CCM does not apply even in our nearest neighbors, the Large and Small Magellanic Clouds (LMC and SMC) (Gordon et al. 2003) with metallicities of about 60% and 25% solar, respectively (Russell and Dopita 1992).

Some of the LMC lines of sight are very CCM-like while those near the giant star-forming region, 30 Dor, have weaker 2175 Å bumps and steeper far-UV extinction. The extinction curves measured for SMC lines of sight are even more extreme. With the exception of one CCM-like sightline, the SMC dust extinction displays very steep far-UV extinction and weak or absent 2175 Å bumps. The most likely explanation for these differences is metallicity variations, whereby lower metallicity means fewer metals available to make the grains. The gas-to-dust ratio is also higher in the LMC and SMC.

Only two lines of sight in the LMC have so far been observed in UV polarization (Clayton et al. 1996). Both of these have small values of λ_{max}. While the uncertainties in the these observations are relatively high both lines of sight are consistent with super-Serkowski behavior. There are no UV polarimetry data for stars in the SMC.

With *Polstar*, significant samples of UV spectropolarimetry of lines of sight in the LMC and SMC will be possible. Such observations will be key to determining how metallicity affects the nature of interstellar dust grains. At least a dozen stars in the SMC and several dozen in the LMC can be observed to the required accuracy with *Polstar*.

2.5.5 Interstellar atomic alignment

In a way conceptually similar to dust grain alignment, atoms and ions with a net angular momentum (i.e., fine structure transitions) are aligned in a magnetic field by anisotropic radiation, called "Ground State Alignment" (GSA; Yan and Lazarian 2006, 2012; Happer 1972). The GSA effect has been seen in a circumstellar region (Zhang et al. 2020), but not yet detected in the diffuse ISM. Spectropolarimetry from GSA is used to measure the scattering geometry, and in some cases the ISM magnetic field and its temporal variations (Yan and Lazarian 2008; Andersson et al. 2022). This informs the baryonic cycle by helping to understand ISM magnetization, energization, and irradiation.

A significant number of well-known UV lines from C I, C II, S I, S II, and Si II are predicted (Yan and Lazarian 2012) to show polarization at the 5–25% level, and testing this, probe magnetism in the diffuse ISM. No previous UV spectropolarimetry mission has had the capability to detect this feature.

2.6 The interface at protoplanetary disks

When ISM material is incorporated into star formation, angular momentum conservation requires that the accretion occurs in a generally disk-like structure. A natural byproduct is the creation of protoplanets, so the final stage in the interface between stars and the ISM is a protoplanetary disk. *Polstar* studies the transition between the two main types of protoplanetary disk accretion described below, spanning intermediate-mass B and A stars, and the transient phenomena in these accretion disks that affect planet building.

Herbig Ae/Be systems are UV bright, A- or B-type pre-main sequence stars of intermediate masses (2-8 M_{sun}) that link high and low-mass stars in pre-Main Sequence evolution (Waters and Waelkens 1998). Current data are insufficient to discriminate between competing accretion models for these masses (Mendigutía et al. 2017). Ongoing *HST* UV treasury surveys (e.g., *HST/Ulysses*) focus on lower-mass, T Tauri systems, which are thought to undergo magnetic accretion. This leaves unanswered the question of how

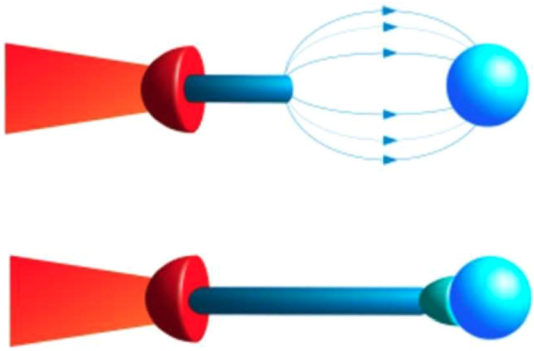

Fig. 8 Where Star Building Meets the Star. Magneto-accretion (top) vs boundary layer interface (bottom) scenarios to be tested with *Polstar*: disk is left in red; star is blue at right. UV spectropolarimetric data can pinpoint the mechanism of mass delivery between the disk and the protostar (Mendigutía 2020)

and where the transition to boundary-layer accretion occurs, and its relevance to higher-mass systems. Near- and mid-IR interferometry can diagnose the innermost (<few au) regions of Herbig disks (Gravity Collaboration et al. 2019; Perraut et al. 2016; Mendigutía et al. 2017; Hone et al. 2019; Labdon et al. 2019; Kluska et al. 2020; Varga et al. 2021; Kokoulina et al. 2021), but deriving detailed nonaxisymmetric structure from near-IR and mid- IR interferometry is challenging (Kluska et al. 2020). Simplifying assumptions are often required during image reconstruction and geometric model fitting (Gravity Collaboration et al. 2019; Kluska et al. 2020), and interferometric techniques cannot resolve the innermost layers where the final stages of accretion occur, important for planet building and the boundary of the forming star. Only UV spectropolarimetry allows observations right down to the stellar surface (Wisniewski et al. 2022) (c.f., Fig. 1(A)), the ultimate destination of ISM/stellar interaction.

2.6.1 The accretion process

Stellar accretion is a fundamental process that connects with the evolutionary status of young disks (Najita et al. 2007; Hartmann et al. 1998) and impacts disk dissipation timescales (Manara et al. 2020). Accretion transpires in the innermost (<few au) regions of Herbig Ae/Be disks. Magnetospheric Accretion (MA) describes the flow of disk material onto lower-mass (< 2 M_{sun}) stars (Bouvier et al. 2007), while boundary layer (BL) accretion (Mendigutía 2020) is believed to be the dominant accretion mechanism for higher-mass stars that have usually transitioned to being nonmagnetic due to their radiative envelopes (Fig. 8).

The mass threshold between MA and BL accretion remains uncertain, but is inferred to happen in the Herbig Ae/Be domain (Vink et al. 2003; Hubrig et al. 2013; Alecian et al. 2013; Mendigutía et al. 2011; Ababakr et al. 2017; Moura et al. 2020; Wichittanakom et al. 2020). Derived accretion rates, hence the size of disk gas reservoirs, change by $2-30\times$ depending on the process, which challenges our understanding of disk evolution (Mendigutía 2020; Wisniewski et al. 2022). *Polstar* establishes the stellar mass where MA accretion transitions to BL accretion, placing low-mass MA accretion, and the building of solar systems like ours, into the context of planet building processes driven by BL accretion.

2.6.2 Protoplanetary transients

Inner disk regions also include the transition from the ionized accretion zone to "dead zones" beyond the accretion regions where most planets are thought to form or to migrate (Mordasini et al. 2009a,b). Based on variability studies, these inner few-au disk regions are highly structured, yet their geometry remains poorly constrained (Kobus et al. 2020; Debes et al. 2017; Tannirkulam et al. 2008; Kóspál et al. 2012; Mendigutía et al. 2013; Morales-Calderón et al. 2011; Rebull et al. 2014; Rodriguez et al. 2017; Flaherty et al. 2016; Kluska et al. 2020). Mis-aligned/warped inner disks and inflated disk walls, inferred from variability studies (Wisniewski et al. 2008; Rich et al. 2019; Ansdell et al. 2020; Benisty et al. 2018; Zhu 2019; Kuffmeier et al. 2021; Rodriguez et al. 2017; Kluska et al. 2020), have been attributed to dynamical sculpting from planets (Ansdell et al. 2020; Benisty et al. 2018; Zhu 2019; Kluska et al. 2020), byproducts of accretion (Ansdell et al. 2020; Kuffmeier et al. 2021), or stellar (Catala et al. 1987; Praderie et al. 1986; Bouret et al. 1997) or disk emission (Sitko et al. 2008). *Polstar* maps the time evolution of the geometry of the inner (<few au) regions of planet-forming disks, to discriminate between competing mechanisms that drive observed variability, to help identify structures that correlate with active planet formation; §2.7.4.

We use time domain UV spectropolarimetry to determine the geometry and physical conditions of regions inside the sublimation zone of the disk (< 0.1 to ~ 1.5 au), to differentiate between competing models (Wisniewski et al. 2022). Because the dominant opacity source changes from equatorial (disk) scattering to polar scattering between the optical and the UV (Whitney et al. 2003b,a, 2004, 2013), UV polarimetry is adept at constraining the geometry of inner circumstellar environments (Bjorkman et al. 1995; Schulte-Ladbeck et al. 1992; Bjorkman 2000; Wisniewski et al. 2022); see also Fig. 9, middle panel).

2.6.3 MA vs. BL accretion

MA is characterized by a truncated inner disk with accretion funnels bringing material to hot spots at high latitude, whereas the emitting region of BL accretion should extend

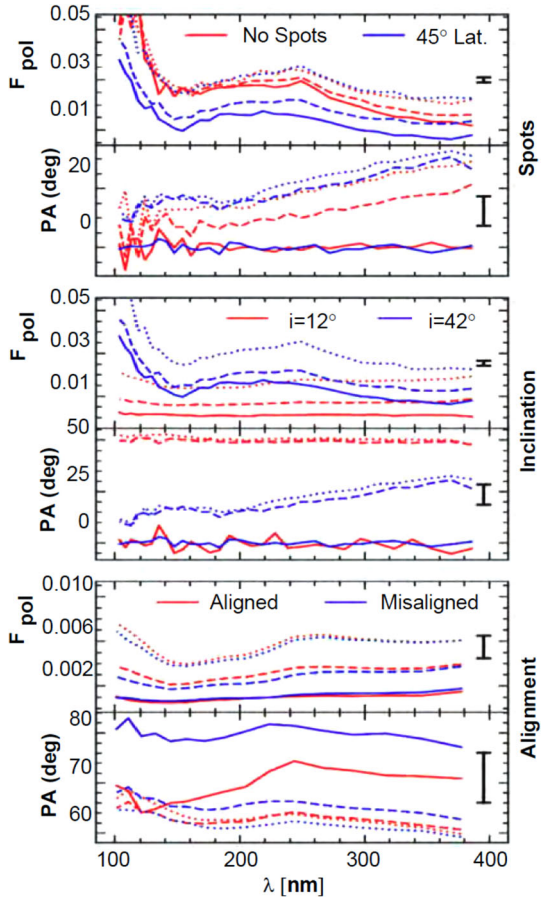

Fig. 9 Polarimetric Mapping of Inner Disks. The amplitude and wavelength dependence of UV fractional polarization and Position Angle (PA) exhibit distinctive trends for different accretion hot spot models, inclinations, and aligned/mis-aligned inner disks, including different evolution over time (depicted by solid, dashed, dotted lines). The amplitudes of these trends will be easily discernible with *Polstar* at 1×10^{-3} precision based on our exposure times and/or binning

to the star in an equatorial annulus (Fig. 8). MA exhibits different time-dependent geometry as compared to BL accretion. We can model the time and wavelength dependence of the continuum polarization and polarization PA with 3D Monte Carlo Radiative Transfer (MCRT) radiative transfer codes such as *HoCHUNK3D* (Whitney et al. 2013) and *RADMC-3D* (Dullemond et al. 2012) to predict full SEDs and polarization for a range of viewing angles.

Using known properties of our well-studied targets to minimize degeneracies, model grids sample a range of inner disk radii and accretion hot spot number and latitude to compare against predictions for MA vs. BL accretion. Predicted UV continuum fractional polarization and PAs for accretion-spot free systems (BL) exhibit different amplitude and time-dependent behavior than MA systems, at levels that significantly exceed a 1×10^{-3} polarization precision (c.f., Fig. 9, top panel; also (Wisniewski et al. 2022)).

The ratio between UV and Balmer Jump excesses is predicted to be different for BL vs MA models for a given star (e.g., Figs. 4-5 in (Mendigutía 2020)). *Polstar*'s spectrophotometric capabilities and observing cadence allows us to simultaneously measure the UV excess across the continuum, accretion-sensitive lines (Mg II, CIV), and the Balmer Jump to test BL vs MA predictions (Mendigutía 2020).

2.6.4 Inner disk dynamics

Mis-aligned inner disks produce periodic wavelength-dependent polarization and PA variability (Fig. 9, bottom panel; also Wisniewski et al. (2022)), and also on the timescales of our observations, inner-disk wall inflation and a disk wind could vary. Collectively, our time series data discriminates between competing models for transient events in the inner (<few au) regions of protoplanetary disks: inner disk misalignments and stellar (or disk) emission.

We quantify the amplitude, time dependence, and wavelength dependence of variable continuum polarization, continuum polarization PA, and UV-optical continuum flux for Ch2 observations of each target. Similarly, we quantify variability in line profiles, velocities, and line strengths of wind lines (e.g., NV 124 nm, SiIV 140 nm, CIV 155 nm, FeIII 190 nm) from Ch1 spectra. The circumstellar regions are localized based on the variability timescale, as corresponding to orbital periods at radii of 0.1- 1.5 au. The Ch1 observations map the type of stellar wind/chromospheric variability that has been observed by *IUE* for AB Aur (Catala et al. 1987) across our target list.

Determining the detailed inner geometry is enabled by comparing the time-dependent polarization and PA to detailed 3D MCRT models (Whitney et al. 2013; Dullemond et al. 2012; Wisniewski et al. 2022) that include the effects of mis-aligned inner disks, inflated disk walls, and disk winds.

3 Science instrumentation

The *Polstar* Instrument provides unprecedented resolving power and effective area for a polarimeter in the FUV and NUV bands. The Telescope uses a demonstrated, space-flight design with axial symmetry and maximized clear aperture. Advances in UV mirror coating uniformity and higher responsivity detectors enable spectropolarimetry (all 4 Stokes parameters) of massive stars with time domain observations.

The instrument combines advances in high reflectivity UV coatings and delta-doped CCDs with high quantum efficiencies to provide dedicated FUV spectropolarimetry for the first time in 25 years. The FUV channel (Ch1), covers 122-200 nm at resolution R=30k, while the NUV channel (Ch2) covers 122-320 nm at R 140-4k, each with the effective areas shown in Fig. 10.

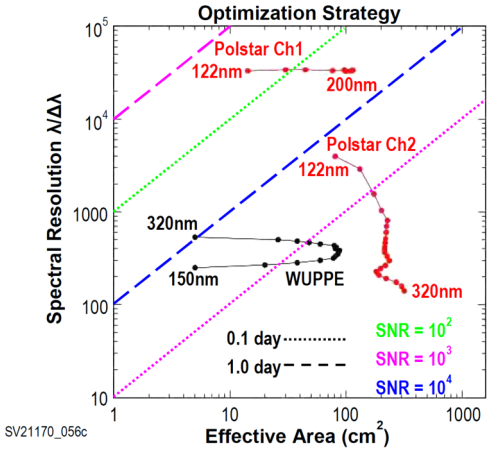

Fig. 10 Advances in Spectropolarimetry. Comparison of effective areas and resolving power of *Polstar*'s Ch1 and Ch2 against previous space-borne polarimeter *WUPPE*. The numbers by the round markers are wavelengths. Line type and colors for diagonal lines are combinations of SNR and average total observation time per target to demonstrate feasibility

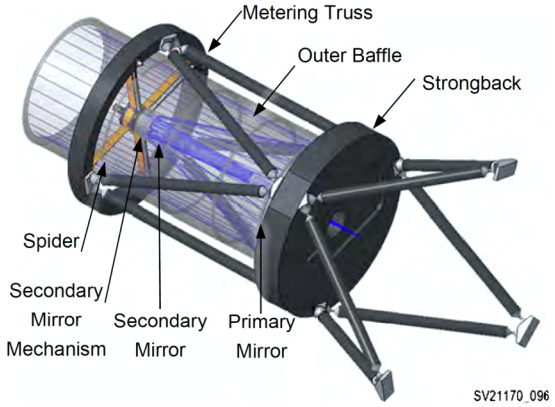

Fig. 11 Optical Telescope Assembly. The metering structure in combination with the strongback provide a very stable optical front end to the *Polstar* instrument. The baffle is separate from the structure and the overall optical system is completely symmetric to minimize the instrumental polarization forward of the entrance slit of the spectrometer

The instrumental polarization stability is built to provide signal-to-noise ratios (SNR) for UV polarimetry precision of 1×10^{-3} per exposure per resolution element (resel). Precision can be further improved with spectral binning and/or stacking multiple exposures. *Polstar* spectral resolution in Ch1 is $> 30\times$ better than *WUPPE*, with $10\times$ better effective area, while reaching shorter wavelength than *WUPPE* (Fig. 10) to access strong lines of species like NIV and SiIV. The 3-year mission of *Polstar* is $100\times$ longer than *WUPPE* with orders of magnitude gains in stellar and interstellar observations.

The diagonal lines demonstrate feasibility of our observation plan. Each color is for a fixed SNR value, and each line type an observing time on target. Spectroscopic studies frequently seek SNR$\sim 1 \times 10^2$ (green), whereas polarimetry requires SNR$\sim 1 \times 10^3$ (magenta). Stacking and spectral binning can increase SNR to higher precision when needed (e.g., 1×10^4, blue). The two line types represent fiducials of 0.1 d (dotted) and 1.0 d (dashed) on-target time for 10 visits. With ~800 total targets, each seeking polarimetry with 1-30 visits, *Polstar* design can achieve the science within the 3-year mission, with 30-40% observing efficiency as margin.

The *Polstar* instrument consists of a two channel Spectropolarimeter (PSP) with a 600 mm Optical Telescope Assembly (OTA) (Fig. 11). The two PSP channels share the OTA, Entrance Slit (ES), Shutter, Polarimeter Assembly (PolA) and science Focal Plane Array (FPA) to provide precision (0.0001) spectral measurements of all four Stokes parameters. Channel 1 (Ch1) is a high-resolution (R> 30k) FUV (122–200 nm) spectropolarimeter used primarily for massive star science. The design is based on GHRS and STIS. Channel 2 (Ch2) is a low-resolution (R=140–4000) FUV/NUV spectropolarimeter for interstellar continuum polarization science (122–320 nm) and spectroscopy from 115– 1000 nm. The channels operate sequentially being selected by a Channel Selector Mirror. The FPA records the PolA modulated spectropolarimetric signals of either selected channel.

3.1 Instrument requirements and design

Table 1 outlines the driving requirements of the instrument design to meet the demands of the science objectives. The *Polstar* design provides precise linear and circular polarimetry based on these requirements. The *Polstar* instrument is comprised of a spectropolarimeter and a telescope as shown in Fig. 12. Elements for the instrument are shown in the block diagram Fig. 13.

3.2 Optical Telescope Assembly (OTA)

If the Stokes vector $S_S = (I, Q, U, V)^T$ represents the stellar source polarization, the OTA must preserve S_S accurately up to the PolA. This requires OTA axial symmetry in physical properties including special constraints on coating reflectance uniformity and mirror surface figure errors. A dual-beam demodulation approach is insensitive to errors introduced by optics after the PolA Wollaston Prism (WP).

The OTA provides uniform, symmetric light while minimizing the number of reflections. The 600 mm diameter parabolic primary mirror (PM) is no faster than f/2 to control polarization effects. The hyperbolic secondary mirror (SM) is supported by a 4-arm spider providing aperture symmetry. The PM and SM substrates are low coefficient of thermal expansion (CTE) ZERODUR® substrates and are coated with FUV/NUV high-efficiency, Lyman-α-enhanced Al+MgF_2 (Quijada et al. 2014). Coatings of these kinds

Table 1 *Polstar* Instrument Design Requirements. The science goals and objectives of the mission are summarized here and feed directly into both the instrument and observatory design

Item	Requirement
Telescope	Axial Symmetry
F-number (minimize depolarization)	≥ f/13 (CLASP, DKIST similarity)
Spectropolarimeter	2 Channels
Wavelengths	Ch1: Polarimetry 122–200 nm
	Spectroscopy 121.4-200.3 nm
	Ch2: Polarimetry 122–300 nm
	Spectroscopy 115–1000 nm
	FGS: Guidance 500–1000 nm
Ch 1 Spectral Resolving Power	R ≥ 30,000 (2.5 pixel)
Ch 2 Spectral Resolving Power	R ≥ 140 at 320 nm (2.5 pixel)
Polarization Precision	≤ 0.0001
Polarimetric Accuracy	≤ 0.001
Signal-to-Noise Ratio	Ch1: 100 to 300 over 600 s
	Ch2: 1300 at 217.5 nm over 600 s
Polarimeter Assembly (PolA)	Measures 4 Stokes parameters
Polarization Calibration	Full characterization on ground
Exposure Time (6× sub-exposures)	100 ms – 600 s
Image Drift at CCD per exposure	≤ 0.1 pixel motion/600 s
Image Jitter at ES per sub-exposure	≤ 0.1 ES diameter motion
FGS FOV	≥ 8 arcmin diameter
Sun Avoidance Angle	≥ 95 degrees

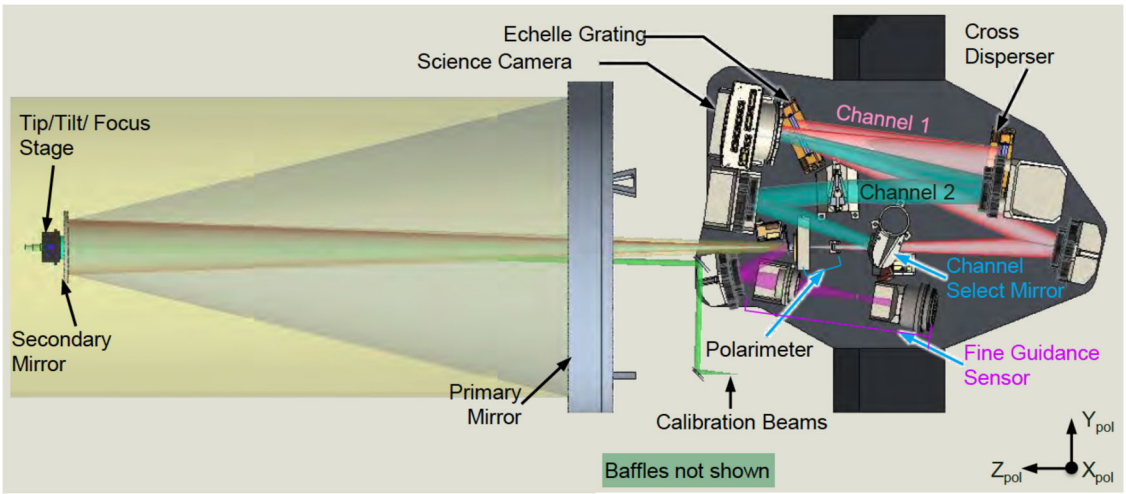

Fig. 12 *Polstar* Instrument Design. The opto-mechanical design uses an ultra-stable optical bench to provide a repeatable measurement from modulator position to modulator position, and is kinematically mounted to the strongback of the telescope. Additional pointing control is provided by an actuated secondary that aids with the spacecraft pointing system and control which is fed by the FGS at the slit entrance

have been demonstrated on mirrors as large as 50 cm recently (Balasubramanian et al. 2017). A 400 mm back focal distance provides ample packaging volume to attach the PSP to the OTA Strongback. OTA baffles limit light to on-axis rays. The OTA Cassegrain focus is at the 793 mas diameter ES. The f/13 beam then propagates onto the PolA. Note that the OTA F-number is selected to match heritage PolA designs (Ishikawa et al. 2015; Snik et al. 2012).

3.2.1 OTA optomechanical design

The OTA shown in Fig. 11 mounts to the Spacecraft (S/C) using a 6-strut system. The PM mounts with 3-bipods to the Strongback optical bench. The Strongback supports the low-

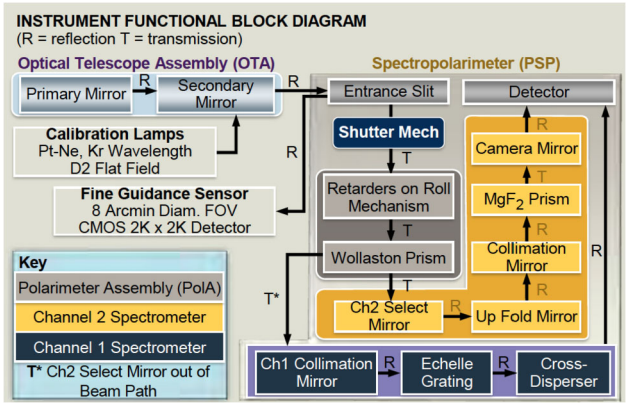

Fig. 13 *Polstar* Instrument Block Diagram. The OTA collects light with a symmetric optical design that minimized instrumental polarization and delivers that light to the entrance slit. Calibration lamps are mounted in the secondary shadow to feed the optical instrument. A mechanical shutter controls light entering the instrument, and the slit has a silvered back to allow the field to be used for guidance via the FGS. The light passes through a rotating modulator and is split by the prism to deliver a two-beam optical encoding of the polarimetric signal, which is then dispersed by either channel and recorded at the detector

CTE composite metering structure providing the SM Assembly (SMA) with stable optical alignment across operational temperatures. Kinematic design principles are used to prevent distortion of critical assemblies in the OTA and PSP. The SMA includes the SM Mechanism (SMM) that has tip, tilt, and focus functionality. The OTA tip/tilt adjustment is used in closed-loop LOS drift control. The OTA focus adjustment is used periodically on-orbit. It may also be used during thermal vacuum testing and post-launch realignment. The 4-arm spider attaches the SMA assembly to a ring structure. A concave spherical mirror is mounted in the central obscured region of the SM to image the input of the calibration light sources to the PSP.

3.3 PSP optomechanical design

Inside the PSP are the ES and the PolA. The ES is a 30 μm diameter (793 mas in object space) pinhole whose diameter equals the image size of the 2.5 px FPA sampling in Ch1 and Ch2. This ES width ensures spectral purity and FPA pixel sampling determines spectral resolving power. The PolA modulates the polarization of the incident signal from the OTA with a rotating modulator and a fixed WP. The PolA optics are single-crystal MgF_2 – the only material that is both birefringent and transparent in the FUV. The modulator uses two retarders, each made of two thin plates. The effective thickness of each retarder is the difference of the individual plate thicknesses (Tomczyk et al. 2010; Pertenais et al. 2015).

A polychromatic retarder design (del Toro Iniesta and Collados 2000) optimizes the effective thickness of each retarder and the clocking angle between the fast axes of the two retarders for polarization recovery efficiency. The modulator mechanism rolls the retarder pair assembly about the OTA optical axis to modulate the stellar polarization. This signal transmits through the fixed WP analyzer, splitting it into two orthogonal polarization states (s and p), thereby introducing angular offsets between the two states in the cross-dispersion direction of the PSP. The internal angle of the WP is optimized to minimize astigmatic differences of the two offset polarimetric images at the FPA (Nikzad et al. 1994; Hoenk et al. 1993).

During an exposure, the retarder plates are rotated as a unit to each of six equidistant azimuth angles between 0° and 180°. The outputs from the analyzer form two displaced spectra on the FPA. An exposure is comprised of six sub-exposures, one at each modulator position.

Extracting Stokes profiles from the six modulator sub-exposures requires the full width at half max (FWHM) of narrow lines to be precise to 0.1 pixel (px) to enable polarimetric measurements with a precision of 10^{-3} for stars with v sin(i) down to ~ 5 km/s. Therefore, the PSP optical alignment must be stable over six sub-exposures.

The PolA crystals are mounted with flightheritage LM optical mounts attached to a (*HMI, IRIS*) flight-heritage hollow core rotary motor. In the baseline design, the modulator is mounted with gaps between each plate. A Phase A study will consider optically contacting each pair to increase throughput while minimizing Fresnel reflections.

The two-retarder pair modulator has polarization recovery efficiency of 50–70% over 122-320 nm and the transmission is 25–75% with gaps.

3.3.1 Channel 1 spectrometer

The Ch1 all-reflective, cross-dispersed, echelle spectrometer design is similar to those in *HST/GHRS* and *HST/STIS* instruments (Fig. 14). The optical path exits the PolA and goes to the Collimating Mirror (CM), then the Echelle Grating (EG), the Cross Disperser (CD) and finally to the FPA.

The EG is a custom Richardson Grating® master with 50° blaze angle and 180 grooves/mm. To minimize scattered light, the design uses a holographically written, blazed, CD (made by Zeiss) with 1000 mm concave spherical radius and 900 grooves/mm with 4.2° blaze angle. It is used in first order in a Wadsworth configuration to control coma over the spectral range (7.71° Wadsworth angle). The CD images the two polarization states from the WP as interleaved echellograms (orders 42 through 69) on the FPA. The minimum order separation is 910 μm (76 px). The separation of the two imaged polarization states is ∼210 μm (18 px) and is sufficient to record both polarization signals without interference with adjacent orders.

The resolving power (R) is R ∼ 34k with 2.5 px sampling at the mid-wavelength of each echelle order, and R > 32k across the full spectral range.

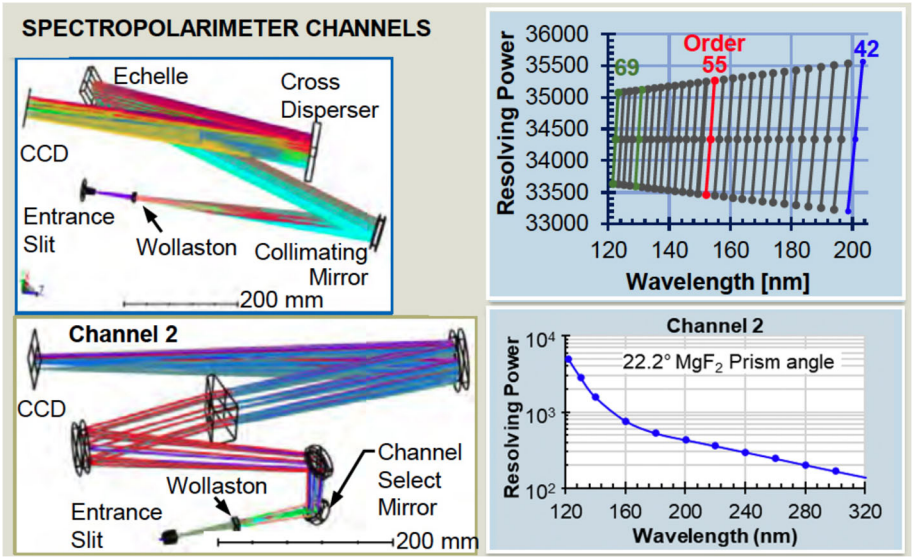

Fig. 14 *Polstar* Spectropolarimeter Channels. The two spectrscopic channels provide very different dispersion, with Channel 1 delivering R=30k FUV spectra using an Echelle combined with a cross-disperser, whereas Channel 2 provides much coarser R=20-200 NUV spectra using a fused silica prism. Multiple orders are recorded at the detector using better than Nyquist sampling across the full bands

3.3.2 Channel 2 spectrometer

Ch2 also uses the PolA. Ch2 is activated when a Channel Selector Mirror (CSM) is rotated into the optical path after the WP. When the CSM is in the beam, it directs light to the Up Fold Mirror (UFM) then to the Ch2 CM, the MgF_2 prism disperser, and then the Camera Mirror which images the s- and p-polarization as displaced linear spectra on the FPA. This lower-resolution spectrometer uses a prism disperser: a 22.2° apex angle MgF_2 prism mounted at minimum deviation to minimize astigmatism.

The design achieves R ∼140 at 320 nm, sampled by 2.5 px (Fig. 14) and varies from R ∼ 16 at 800 nm to ∼ 4 K at 120 nm.

From optical analysis, at the closest spacing (122 nm), the separation between s and p polarization images is 300 μm center-to-center.

The PSP includes stray light baffles to prevent the FPA from viewing directly illuminated surfaces. Also, a zero-order trap captures the zero-order image of the CD.

3.3.3 Science focal plane and camera

A key enabling technology for *Polstar* is the large format, delta-doped, Teledyne e2V CCD272-84, a simplified design from Euclid's CCD273 detector. These detectors are procured by JPL, who process fully fabricated Teledyne-e2V CCD272-84 wafers to enhance UV sensitivity and stability. JPL's 2D, or "delta" doping process uses molecular beam epitaxy (MBE) to create a highly stable, ultrathin layer of high concentration dopant near the backside CCD surface, providing 100% internal quantum efficiency (QE) across UV and visible wavelengths. Anti-reflection coatings are then added via atomic layer deposition (ALD) to tailor the QE to the desired bandpass (Kyne et al. 2016; Nikzad et al. 2017; Jelinsky et al. 2003). JPL deposits an anti-reflection coating directly onto the silicon (Wong et al. 2009) to further boost throughput from 122–320 nm. The resulting instrument achieves high QE without the hysteresis observed in other UV CCDs (e.g., HST/WFC3; van Bezooijen (2003), Sanders (2010)).

3.4 Instrument calibration plan

A detailed set of calibration activities are outlined to ensure meeting the science goals. Spectral Calibration uses a Pt/Ne hollow cathode wavelength calibration lamp (Kerber et al. 2004) and ISM atomic absorption lines calibrate the pixel to wavelength FPA locations. Photometric and flat field calibration use a combination of Kr and D_2 lamps, or external standard stars, with continuum spectra over the spectral range. FPA characterizations include QE, linearity, dark current, read noise, amplifier gains, and charge transfer inefficiency measurements. Locations of bad pixels and columns are noted. Throughput and wavelength response at the component level are measured and confirmed with an end-to-end test in the Thermal Vacuum (TVAC) chamber. Expected effective areas including throughput are shown in Fig. 15. For polarization calibration, the Mueller matrices for the PSP and OTA are estimated across the full spectral region prior to launch.

The Polarization Calibration Source (PCS) is a piece of ground support equipment (GSE) that generates highly polarized state inputs. Across the full spectral region, the PCS provides three essential functions. The PCS produces light of known Degree of Polarization (DoP) where $\delta = 1 - \text{DoP} \leq 10^{-5}$ for both linear and circular polarizations meeting the *Polstar* polarization precision error budget (Table 2). It images the converging polarized beam at f/13 to properly mimic the optical beam between the OTA and PSP. It allows

Table 2 The *Polstar* polarization error budget demonstrates that the instrument design meets the necessary accuracy requirements with plenty of margin

Item	1 – DoP	Error Allocated
Polarization Accuracy Requirement	1.00×10^{-3}	
Linear Margin	1.93×10^{-4}	
Estimated Polarization Accuracy	8.07×10^{-4}	
Reflections/scatter from baffle (PM&SM)		5.20×10^{-4}
Spatial variation of FPA response		5.01×10^{-5}
Modulator errors (wobble, repeatability)		5.54×10^{-6}
OTA coating refl.& phase nonuniformity		6.12×10^{-4}
OTA particulates contamination		5.66×10^{-5}
OTA slope and PM/SM tilt errors		1.57×10^{-6}
SC body point uncertainty		1.10×10^{-6}
Ground calibration error		1.00×10^{-5}

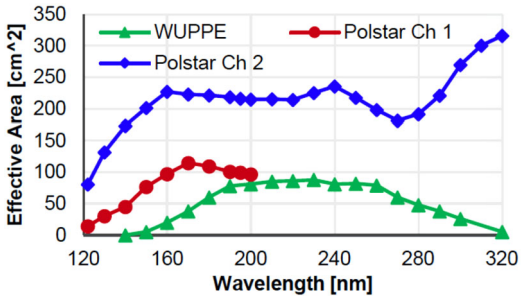

Fig. 15 *Polstar* expected effective area is sufficient to meet the science mission goals, and is a dramatic increase over its predecessors. Combined with advances in detectors, mirror coatings and grating technologies *Polstar* delivers orders of magnitude improvement, see Fig. 10

full characterization of the PSP and provides 360° azimuthal roll of the state relative to the WP axis.

FUV/NUV lamps (D_2, Kr, Pt/Ne HCL) are injected into an integrating sphere (IS) of the PCS. The IS provides an unpolarized light source that covers the full wavelength range.

4 Summary

The *Polstar* mission design and science program represent the convergence of new advances achieved via technological investment development in the ultraviolet for detectors and coatings, combined with advances in polarimeter design, and scientific advances in the knowledge and understanding of the environments of massive stars, the interstellar medium, and the formation of protoplanetary systems. *Polstar* will return the capability of FUV spectropolarimetry to the astronomical community after a 25 year absence, and do it with orders of magnitude improvement in the combination of sensitivity and spectral resolution, while delivering unprecedented polarimetric accuracy in the diagnostic-rich domain of the ultraviolet. The mission is responsive to priorities identified in both the 2010 and 2020 Decadal Surveys that outlined the need for a better understanding of the influence of stellar environment and structure on the ultimate evolution of the single class of star that most influences the baryonic cycle and shapes the stellar, planetary and chemical evolution of galaxies.

Author Contribution KG and RI both contributed substantially to §2 and §4. GV and RW contributed substantially to §3. CN and RC contributed to §3 and §4. MS contributed to §4.5. BA contributed to §4.6. JW contributed to §4.7.

Funding RI gratefully acknowledges support by the National Science Foundation under Grant No. AST-2009412. PS acknowledges support by both Arizona State University and then by NASA as a civil servant during the completion of this work. The material provided by RC is based upon work supported by the National Center for Atmospheric Research, which is a major facility sponsored by the National Science Foundation under Cooperative Agreement No. 1852977. B-GA. gratefully acknowledges the support of the National Science Foundation under grant AST-1715876, as well as USRA corporate sponsorship.

Data Availability No data will be generated by the work in this paper.

Declarations

Conflict of Interest None known.

References

Ababakr, K.M., Fairlamb, J.R., Oudmaijer, R.D., et al.: Spectroscopy and linear spectropolarimetry of the early Herbig Be stars PDS 27 and PDS 37. Mon. Not. R. Astron. Soc. **452**(3), 2566–2578 (2015). https://doi.org/10.1093/mnras/stv1483. arXiv:1507.06313 [astro-ph.SR]

Ababakr, K.M., Oudmaijer, R.D., Vink, J.S.: A statistical spectropolarimetric study of Herbig Ae/Be stars. Mon. Not. R. Astron. Soc. **472**(1), 854–868 (2017). https://doi.org/10.1093/mnras/stx1891. arXiv:1707.08408 [astro-ph.SR]

Alecian, E., Wade, G.A., Catala, C., et al.: A high-resolution spectropolarimetric survey of Herbig Ae/Be stars – I. Observations and measurements. Mon. Not. R. Astron. Soc. **429**(2), 1001–1026 (2013). https://doi.org/10.1093/mnras/sts383. arXiv:1211.2907 [astro-ph.SR]

Anderson, C.M., Weitenbeck Astron, J., Code, A.D., et al.: Ultraviolet interstellar polarization of galactic starlight. I. Observations by the Wisconsin ultraviolet photo polarimeter experiment. Astron. J. **112**, 2726 (1996). https://doi.org/10.1086/118217

Andersson, B., Clayton, G., Doney, K., et al.: Ultraviolet Spectropolarimetry with Polstar: Interstellar Medium Science. Astrophys. Space Sci. **367** (2022). https://doi.org/10.1007/s10509-022-04153-3

Andersson, B.G., Lazarian, A., Vaillancourt, J.E.: Interstellar dust grain alignment. Annu. Rev. Astron. Astrophys. **53**, 501–539 (2015). https://doi.org/10.1146/annurev-astro-082214-122414

Andrews, S.M.: Observations of protoplanetary disk structures. Annu. Rev. Astron. Astrophys. **58**, 483–528 (2020). https://doi.org/10.1146/annurev-astro-031220-010302. arXiv:2001.05007 [astro-ph.EP]

Ansdell, M., Gaidos, E., Hedges, C., et al.: Are inner disc misalignments common? ALMA reveals an isotropic outer disc inclination distribution for young dipper stars. Mon. Not. R. Astron. Soc. **492**(1), 572–588 (2020). https://doi.org/10.1093/mnras/stz3361. arXiv:1912.01610 [astro-ph.EP]

Balasubramanian, K., Hennessy, J., Raouf, N., et al.: Mirror coatings for large aperture UV optical infrared telescope optics. Society of Photo-Optical Instrumentation Engineers (SPIE) Conference Series p. 103980X (2017). https://doi.org/10.1117/12.2274794

Beck, R., Brandenburg, A., Moss, D., et al.: Galactic magnetism: recent developments and perspectives. Annu. Rev. Astron. Astrophys. **34**, 155–206 (1996). https://doi.org/10.1146/annurev.astro.34.1.155.

Benisty, M., Juhász, A., Facchini, S., et al.: Shadows and asymmetries in the T Tauri disk HD 143006: evidence for a misaligned inner disk. Astron. Astrophys. **619**, A171 (2018). https://doi.org/10.1051/0004-6361/201833913. arXiv:1809.01082 [astro-ph.EP]

Bjorkman, J.E., Ignace, R., Tripp, T.M., et al.: Evidence for a disk in the wind of HD 93521: UV line profiles from an axisymmetric model. Astrophys. J. **435**, 416 (1994). https://doi.org/10.1086/174825

Bjorkman, K.S.: Polarimetry as a diagnostic of circumstellar envelopes. In: Smith, M.A., Henrichs, H.F., Fabregat, J. (eds.) IAU Colloq. 175: The Be Phenomenon in Early-Type Stars, p. 384 (2000)

Bjorkman, K.S., Meade, M.R., Babler, B.L., et al.: Diagnosing the circumstellar environment of HD163296. In: American Astronomical Society Meeting Abstracts, p. 106.04 (1995)

Bouret, J.C., Catala, C., Simon, T.: Nitrogen V in the wind of the pre-main sequence Herbig AE star AB Aurigae. Astron. Astrophys. **328**, 606–616 (1997)

Bouret, J.C., Lanz, T., Hillier, D.J.: Lower mass loss rates in O-type stars: spectral signatures of dense clumps in the wind of two Galactic O4 stars. Astron. Astrophys. **438**(1), 301–316 (2005). https://doi.org/10.1051/0004-6361:20042531. arXiv:astro-ph/0412346 [astro-ph]

Bouvier, J., Alencar, S.H.P., Harries, T.J., et al.: Magnetospheric accretion in classical T Tauri Stars. In: Reipurth, B., Jewitt, D., Keil, K. (eds.) Protostars and Planets V, p. 479 (2007). astro-ph/0603498

Bowyer, S., Malina, R.F., Lampton, M., et al.: The extreme ultraviolet explorer. In: Hunter, W.R. (ed.) Ultraviolet and Vacuum Ultraviolet Systems, pp. 176–182 (1981). https://doi.org/10.1117/12.965721

Brott, I., de Mink, S.E., Cantiello, M., et al.: Rotating massive main-sequence stars. I. Grids of evolutionary models and isochrones. Astron. Astrophys. **530**, A115 (2011). https://doi.org/10.1051/0004-6361/201016113. arXiv:1102.0530 [astro-ph.SR]

Brown, J.C., Richardson, L.L., Antokhin, I., et al.: Combined spectrometric, photometric and polarimetric diagnostics for 'blobs' in WR star winds. Astron. Astrophys. **295**, 725 (1995)

Butsky, I., Zrake, J., Jh, K., et al.: Ab initio simulations of a supernova-driven galactic dynamo in an isolated disk galaxy. Astrophys. J. **843**(2), 113 (2017). https://doi.org/10.3847/1538-4357/aa799f. arXiv:1610.08528 [astro-ph.GA]

Cantó, J., Raga, A.C., Wilkin, F.P.: Exact, algebraic solutions of the thin-shell two-wind interaction problem. Astrophys. J. **469**, 729 (1996). https://doi.org/10.1086/177820

Cardelli, J.A., Clayton, G.C., Mathis, J.S.: The relationship between infrared, optical, and ultraviolet extinction. Astrophys. J. **345**, 245 (1989a). https://doi.org/10.1086/167900

Cardelli, J.A., Clayton, G.C., Mathis, J.S.: The relationship between infrared, optical, and ultraviolet extinction. Astrophys. J. **345**, 245–256 (1989b)

Catala, C., Praderie, F., Felenbok, P.: Rotational modulation of the wind of the PMS star AB AUR: new observations in C IV and MG II. Astron. Astrophys. **182**: 115–119 (1987)

Clayton, G.C., Green, J., Wolff, M.J., et al.: Astro-2 observations of interstellar dust and gas in the large magellanic cloud. Astrophys. J. **460**, 313 (1996)

Clayton, G.C., Wolff, M.J., Sofia, U.J., et al.: Dust grain size distributions from MRN to MEM. Astrophys. J. **588**(2), 871–880 (2003). https://doi.org/10.1086/374316. arXiv:astro-ph/0301488 [astro-ph]

Cotton, D.V., Bailey, J., Howarth, I.D., et al.: Polarization due to rotational distortion in the bright star Regulus. Nat. Astron. **1**, 690–696 (2017). https://doi.org/10.1038/s41550-017-0238-6. arXiv:1804.06576 [astro-ph.SR]

Cranmer, S.R., Owocki, S.P.: Hydrodynamical simulations of corotating interaction regions and discrete absorption components in rotating O-star winds. Astrophys. J. **462**, 469 (1996). https://doi.org/10.1086/177166. arXiv:astro-ph/9508004 [astro-ph]

Davidsen, A.F., Fountain, G.H.: The Hopkins ultraviolet telescope. Johns Hopkins APL Tech. Dig. **6**, 28–37 (1985)

Davies, B., Vink, J.S., Oudmaijer, R.D.: Modelling the clumping-induced polarimetric variability of hot star winds. Astron. Astrophys. **469**(3), 1045–1056 (2007). https://doi.org/10.1051/0004-6361:20077193. arXiv:0704.2569 [astro-ph]

de Mink, S.E., Langer, N., Izzard, R.G., et al.: The rotation rates of massive stars: the role of binary interaction through tides, mass transfer, and mergers. Astrophys. J. **764**(2), 166 (2013). https://doi.org/10.1088/0004-637X/764/2/166. arXiv:1211.3742 [astro-ph.SR]

Debes, J.H., Poteet, C.A., Jang-Condell, H., et al.: Chasing shadows: rotation of the azimuthal asymmetry in the TW Hya disk. Astrophys. J. **835**(2), 205 (2017). https://doi.org/10.3847/1538-4357/835/2/205. arXiv:1701.03152 [astro-ph.SR]

del Toro Iniesta, J.C., Collados, M.: Optimum modulation and demodulation matrices for solar polarimetry. Appl. Opt. **39**(10), 1637–1642 (2000). https://doi.org/10.1364/AO.39.001637

Dessart, L., Hillier, D.J.: Synthetic line and continuum linear-polarization signatures of axisymmetric type II supernova ejecta. Mon. Not. R. Astron. Soc. **415**(4), 3497–3519 (2011). https://doi.org/10.1111/j.1365-2966.2011.18967.x. arXiv:1104.5346 [astro-ph.SR]

Donati, J.F., Landstreet, J.D.: Magnetic fields of nondegenerate stars. Annu. Rev. Astron. Astrophys. **47**(1), 333–370 (2009). https://doi.org/10.1146/annurev-astro-082708-101833. arXiv:0904.1938 [astro-ph.SR]

Donati, J.F., Semel, M., Carter, B.D., et al.: Spectropolarimetric observations of active stars. Mon. Not. R. Astron. Soc. **291**(4), 658–682 (1997). https://doi.org/10.1093/mnras/291.4.658

Draine, B.T., Fraisse, A.A.: Polarized far-infrared and submillimeter emission from interstellar dust. Astrophys. J. **696**(1), 1–11

(2009). https://doi.org/10.1088/0004-637X/696/1/1. arXiv:0809.2094 [astro-ph]
Dullemond, C.P., Juhasz, A., Pohl, A., et al.: RADMC-3D: a multi-purpose radiative transfer tool (2012). 1202.015
Eggenberger, P., Meynet, G., Maeder, A., et al.: The Geneva stellar evolution code. Astrophys. Space Sci. **316**(1–4), 43–54 (2008). https://doi.org/10.1007/s10509-007-9511-y
Eichler, D., Usov, V.: Particle acceleration and nonthermal radio emission in binaries of early-type stars. Astrophys. J. **402**, 271 (1993). https://doi.org/10.1086/172130
Erba, C., David-Uraz, A., Petit, V., et al.: Ultraviolet line profiles of slowly rotating massive star winds using the 'analytic dynamical magnetosphere' formalism. Mon. Not. R. Astron. Soc. **506**(4), 5373–5388 (2021a). https://doi.org/10.1093/mnras/stab1853. arXiv:2106.13676 [astro-ph.SR]
Erba, C., Petit, V., Gayley, K., et al.: Detecting the Zeeman effect in Massive Star Magnetospheres in the UV (2021b). e-prints arXiv:2107.09007. arXiv:2107.09007 [astro-ph.SR]
Flaherty, K.M., DeMarchi, L., Muzerolle, J., et al.: Spitzer observations of long-term infrared variability among young stellar objects in chamaeleon I. Astrophys. J. **833**(1), 104 (2016). https://doi.org/10.3847/1538-4357/833/1/104. arXiv:1609.09100 [astro-ph.SR]
Folsom, C.P., Ignace, R. Erba, C., et al.: Ultraviolet Spectropolarimetry: Investigating stellar magnetic field diagnostics. Astrophys. Space Sci. **367** (2022). https://doi.org/10.1007/s10509-022-04140-8
Ford, H.C.: Hubble Space Telescope: Faint object spectrograph instrument handbook. Version 1.1 (1990)
Fox, G.K., Henrichs, H.F.: The theoretical correlation between UV discrete absorption components and the polarization of ejected blobs in the winds of early-type stars. Mon. Not. R. Astron. Soc. **266**, 945–952 (1994). https://doi.org/10.1093/mnras/266.4.945
Fullard, A.G.: A spectropolarimetric study of Wolf-Rayet binary stars. PhD thesis, University of Denver, United States (2020)
Gayley, K., Vink, J.S., ud Doula, A., et al.: Understanding Structure in Line-Driven Stellar Winds Using Ultraviolet Spectropolarimetry in the Time Domain. Astrophys. Space Sci. **367** (2022). https://doi.org/10.1007/s10509-022-04142-6
Gayley, K.G.: Asymptotic opening angles for colliding-wind bow shocks: the characteristic-angle approximation. Astrophys. J. **703**(1), 89–95 (2009). https://doi.org/10.1088/0004-637X/703/1/89. arXiv:0905.1395 [astro-ph.SR]
Georgy, C., Ekström, S., Eggenberger, P., et al.: Grids of stellar models with rotation. III. Models from 0.8 to 120 $M_{\odot}$ at a metallicity Z = 0.002. Astron. Astrophys. **558**, A103 (2013). https://doi.org/10.1051/0004-6361/201322178. arXiv:1308.2914 [astro-ph.SR]
Gordon, K.D., Clayton, G.C., Misselt, K.A., et al.: A quantitative comparison of the small magellanic cloud, large magellanic cloud, and milky way ultraviolet to near-infrared extinction curves. Astrophys. J. **594**, 279–293 (2003)
Gravity Collaboration, Perraut, K., Labadie, L., et al.: The GRAVITY young stellar object survey. I. Probing the disks of Herbig Ae/Be stars in terrestrial orbits. Astron. Astrophys. **632**, A53 (2019). https://doi.org/10.1051/0004-6361/201936403. arXiv:1911.00611 [astro-ph.SR]
Green, J.C., Morse, J. (COS Instrument Definition Team): The cosmic origins spectrograph: a 2002 replacement instrument for the hubble space telescope. In: Wamsteker, W., Gonzalez Riestra, R., Harris, B. (eds.) Ultraviolet Astrophysics Beyond the IUE Final Archive, p. 805 (1998)
Grunhut, J.H., Wade, G.A., Neiner, C., et al.: The MiMeS survey of magnetism in massive stars: magnetic analysis of the O-type stars. Mon. Not. R. Astron. Soc. **465**(2), 2432–2470 (2017). https://doi.org/10.1093/mnras/stw2743. arXiv:1610.07895 [astro-ph.SR]
Gull, T.R., et al.: The space telescope imaging spectrograph. In: Rolfe, E.J., Wilson, R. (eds.) New Insights in Astrophysics. Eight Years of UV Astronomy with IUE, p. 653 (1986)
Happer, W.: Optical pumping. Rev. Mod. Phys. **44**(2), 169–249 (1972). https://doi.org/10.1103/RevModPhys.44.169
Harries, T.J., Howarth, I.D.: Linear spectropolarimetry of the Hα emission line of ζ Puppis. Astron. Astrophys. **310**, 533–546 (1996)
Harries, T.J., Babler, B.L., Fox, G.K.: The polarized spectrum of the dust producing Wolf-Rayet+O-star binary WR137. Astron. Astrophys. **361**, 273–282 (2000)
Harries, T.J., Howarth, I.D., Evans, C.J.: Spectropolarimetry of O supergiants. Mon. Not. R. Astron. Soc. **337**(1), 341–355 (2002). https://doi.org/10.1046/j.1365-8711.2002.05926.x
Hartmann, L., Calvet, N., Gullbring, E., et al.: Accretion and the evolution of T Tauri disks. Astrophys. J. **495**(1), 385–400 (1998). https://doi.org/10.1086/305277
Hensley, B.S., Draine, B.T.: Observational constraints on the physical properties of interstellar dust in the post-Planck era. Astrophys. J. **906**(2), 73 (2021). https://doi.org/10.3847/1538-4357/abc8f1. arXiv:2009.00018 [astro-ph.GA]
Hillier, D.J.: The calculation of line polarization due to scattering by electrons in multi-scattering axisymmetric envelopes. Astron. Astrophys. **308**, 521–534 (1996)
Hillier, D.J.: UV spectroscopy of massive stars. Galaxies **8**(3), 60 (2020). https://doi.org/10.3390/galaxies8030060
Hiltner, W.A.: On the presence of polarization in the continuous radiation of stars. II. Astrophys. J. **109**, 471 (1949). https://doi.org/10.1086/145151
Hoang, T., Lazarian, A.: A unified model of grain alignment: radiative alignment of interstellar grains with magnetic inclusions. Astrophys. J. **831**(2), 159 (2016). https://doi.org/10.3847/0004-637X/831/2/159. arXiv:1605.02828 [astro-ph.GA]
Hoenk, M.E., Grunthaner, P.J., Grunthaner, F.J., et al.: Delta-Doped CCDs – Potential New Low Energy Particle Detectors. Tsurutani, B.T. (ed.): pp. 4–29. Small Instruments for Space Physics, Small Instrument Workshop, 29-31 March 1993, in Pasadena, CA; National Aeronautics and Space Division (1993)
Hoffman, J.L., Nordsieck, K.H., Fox, G.K.: Spectropolarimetric evidence for a bipolar flow in beta lyrae. Astron. J. **115**(4), 1576–1591 (1998). https://doi.org/10.1086/300274
Hone, E., Kraus, S., Davies, C.L., et al.: Compact gaseous accretion disk in Keplerian rotation around MWC 147. Astron. Astrophys. **623**, A38 (2019). https://doi.org/10.1051/0004-6361/201834626. arXiv:1901.04394 [astro-ph.SR]
Hubrig, S., Ilyin, I., Schöller, M., et al.: HARPS spectropolarimetry of Herbig Ae/Be stars. Astron. Nachr. **334**(10), 1093 (2013). https://doi.org/10.1002/asna.201311948. arXiv:1307.0133 [astro-ph.SR]
Ignace, R., Nordsieck, K.H., Cassinelli, J.P.: The hanle effect as a diagnostic of magnetic fields in stellar envelopes. IV. Application to polarized P cygni wind lines. Astrophys. J. **609**(2), 1018–1034 (2004). https://doi.org/10.1086/421258. arXiv:astro-ph/0403416 [astro-ph]
Ignace, R., St-Louis, N., Proulx-Giraldeau, F.: Polarimetric modeling of corotating interaction regions threading massive-star winds. Astron. Astrophys. **575**, A129 (2015). https://doi.org/10.1051/0004-6361/201424806. arXiv:1501.07563 [astro-ph.SR]
Ishikawa, R., Trujillo Bueno, J., Uitenbroek, H., et al.: Indication of the Hanle effect by comparing the scattering polarization observed by CLASP in the Lyα and Si III 120.65 nm lines. Astrophys. J. **841**(1), 31 (2017). https://doi.org/10.3847/1538-4357/aa6ca9
Ishikawa, S., Shimizu, T., Kano, R., et al.: Development of a precise polarization modulator for UV spectropolarimetry. Sol. Phys. **290**(10), 3081–3088 (2015). https://doi.org/10.1007/s11207-015-0774-0. arXiv:1509.05716 [astro-ph.IM]
Jelinsky, P.N., Morrissey, P.F., Malloy, J.M., et al.: Performance results of the GALEX cross delay line detectors. In: Blades, J.C., Siegmund, O.H.W. (eds.) Future EUV/UV and Visible Space Astrophysics Missions and Instrumentation, pp. 233–240 (2003). https://doi.org/10.1117/12.460013

Jones, C., Labadie-Bartz, J., Cotton, D., et al.: Ultraviolet Spectropolarimetry: on the origin of rapidly rotating B stars. Astrophys. Space Sci. **367** (2022). https://doi.org/10.1007/s10509-022-04127-5

Kaper, L., Henrichs, H.F., Fullerton, A.W., et al.: Coordinated ultraviolet and Hα spectroscopy of bright O-type stars. Astron. Astrophys. **327**, 281–298 (1997)

Kerber, F., Rosa, M.R., Sansonetti, C.J., et al.: Spectral characterization of HST calibration lamps: new Pt/Cr-Ne line catalogues and aging test. In: Hasinger, G., Turner, M.J.L. (eds.) UV and Gamma-Ray Space Telescope Systems, pp. 679–690 (2004). https://doi.org/10.1117/12.550507

Keszthelyi, Z., Meynet, G., Shultz, M.E., et al.: The effects of surface fossil magnetic fields on massive star evolution – II. Implementation of magnetic braking in MESA and implications for the evolution of surface rotation in OB stars. Mon. Not. R. Astron. Soc. **493**(1), 518–535 (2020). https://doi.org/10.1093/mnras/staa237. arXiv:2001.06239 [astro-ph.SR]

Kluska, J., Berger, J.P., Malbet, F., et al.: A family portrait of disk inner rims around Herbig Ae/Be stars. Hunting for warps, rings, self shadowing, and misalignments in the inner astronomical units. Astron. Astrophys. **636**, A116 (2020). https://doi.org/10.1051/0004-6361/201833774. arXiv:2004.01594 [astro-ph.SR]

Kobus, J., Wolf, S., Ratzka, T., et al.: Interferometric study on the temporal variability of the brightness distributions of protoplanetary disks. Astron. Astrophys. **642**, A104 (2020). https://doi.org/10.1051/0004-6361/202038013. arXiv:2008.08374 [astro-ph.SR]

Kochukhov, O., Makaganiuk, V., Piskunov, N.: Least-squares deconvolution of the stellar intensity and polarization spectra. Astron. Astrophys. **524**, A5 (2010). https://doi.org/10.1051/0004-6361/201015429. arXiv:1008.5115 [astro-ph.SR]

Kokoulina, E., Matter, A., Lopez, B., et al.: First MATISSE L-band observations of HD 179218. Is the inner 10 au region rich in carbon dust particles? Astron. Astrophys. **652**, A61 (2021). https://doi.org/10.1051/0004-6361/202141175. arXiv:2106.12947 [astro-ph.EP]

Kóspál, Á., Ábrahám, P., Acosta-Pulido, J.A., et al.: Mid-infrared spectral variability atlas of young stellar objects. Astrophys. J. Suppl. **201**(2), 11 (2012). https://doi.org/10.1088/0067-0049/201/2/11. arXiv:1204.3473 [astro-ph.SR]

Kudritzki, R.P.: Line-driven winds, ionizing fluxes, and ultraviolet spectra of hot stars at extremely low metallicity. I. Very massive O stars. Astrophys. J. **577**(1), 389–408 (2002). https://doi.org/10.1086/342178. arXiv:astro-ph/0205210 [astro-ph]

Kuffmeier, M., Dullemond, C.P., Reissl, S., et al.: Misaligned disks induced by infall. Astron. Astrophys. **656**, A161 (2021). https://doi.org/10.1051/0004-6361/202039614. arXiv:2110.04309 [astro-ph.SR]

Kyne, G., Hamden, E.T., Lingner, N., et al.: The faint intergalactic-medium red-shifted emission balloon: future UV observations with EMCCDs. In: Holland, A.D., Beletic, J. (eds.) High Energy, Optical, and Infrared Detectors for Astronomy VII, p. 991507 (2016). https://doi.org/10.1117/12.2232879

Labdon, A., Kraus, S., Davies, C.L., et al.: Dusty disk winds at the sublimation rim of the highly inclined, low mass young stellar object SU Aurigae. Astron. Astrophys. **627**, A36 (2019). https://doi.org/10.1051/0004-6361/201935331. arXiv:1905.11907 [astro-ph.EP]

Lancaster, L., Ostriker, E.C., Kim, J.G., et al.: Star formation regulation and self-pollution by stellar wind feedback. Astrophys. J. **922**(1), L3 (2021). https://doi.org/10.3847/2041-8213/ac3333. arXiv:2110.05508 [astro-ph.GA]

Langer, N.: Presupernova evolution of massive single and binary stars. Annu. Rev. Astron. Astrophys. **50**, 107–164 (2012). https://doi.org/10.1146/annurev-astro-081811-125534. arXiv:1206.5443 [astro-ph.SR]

Lazarian, A., Hoang, T.: Radiative torques: analytical model and basic properties. Mon. Not. R. Astron. Soc. **378**(3), 910–946 (2007). https://doi.org/10.1111/j.1365-2966.2007.11817.x. arXiv:0707.0886 [astro-ph]

Li, Q.K., Cassinelli, J.P., Brown, J.C., et al.: Polarization variability arising from clumps in the winds of Wolf-Rayet stars. Res. Astron. Astrophys. **9**(5), 558–576 (2009). https://doi.org/10.1088/1674-4527/9/5/007. arXiv:0903.3082 [astro-ph.SR]

Macchetto, F.: The International Ultraviolet Explorer (IUE). Mem. Soc. Astron. **a47**, 431 (1976)

Manara, C.F., Natta, A., Rosotti, G.P., et al.: X-shooter survey of disk accretion in Upper Scorpius. I. Very high accretion rates at age > 5 Myr. Astron. Astrophys. **639**, A58 (2020). https://doi.org/10.1051/0004-6361/202037949. arXiv:2004.14232 [astro-ph.SR]

Manso Sainz, R., Martínez González, M.J.: Hanle effect for stellar dipoles and quadrupoles. Astrophys. J. **760**(1), 7 (2012). https://doi.org/10.1088/0004-637X/760/1/7. arXiv:1209.6187 [astro-ph.SR]

Martin, P.G., Clayton, G.C., Wolff, M.J.: Ultraviolet interstellar linear polarization. V. Analysis of the final data set. Astrophys. J. **510**(2), 905–914 (1999). https://doi.org/10.1086/306613

Massa, D., Prinja, R.K.: On the origin of wind line variability in O stars. Astrophys. J. **809**(1), 12 (2015). https://doi.org/10.1088/0004-637X/809/1/12. arXiv:1506.06605 [astro-ph.SR]

Mathis, J.S., Rumpl, W., Nordsieck, K.H.: The size distribution of interstellar grains. Astrophys. J. **217**, 425–433 (1977). https://doi.org/10.1086/155591

Mendigutía, I.: On the mass accretion rates of Herbig Ae/Be stars. Magnetospheric accretion or boundary layer? Galaxies **8**(2): 39, (2020). https://doi.org/10.3390/galaxies8020039. arXiv:2005.01745 [astro-ph.SR]

Mendigutía, I., Calvet, N., Montesinos, B., et al.: Accretion rates and accretion tracers of Herbig Ae/Be stars. Astron. Astrophys. **535**, A99 (2011). https://doi.org/10.1051/0004-6361/201117444. arXiv:1109.3288 [astro-ph.SR]

Mendigutía, I., Brittain, S., Eiroa, C., et al.: Accretion variability of Herbig Ae/Be stars observed by X-shooter HD 31648 and HD 163296. Astrophys. J. **776**(1), 44 (2013). https://doi.org/10.1088/0004-637X/776/1/44. arXiv:1308.3248 [astro-ph.SR]

Mendigutía, I., Oudmaijer, R.D., Mourard, D., et al.: The compact Hα emitting regions of the Herbig Ae/Be stars HD 179218 and HD 141569 from CHARA spectro-interferometry. Mon. Not. R. Astron. Soc. **464**(2), 1984–1989 (2017). https://doi.org/10.1093/mnras/stw2515. arXiv:1610.00013 [astro-ph.SR]

Misselt, K.A., Gordon, K.D., Clayton, G.C., et al.: The DIRTY model. II. Self-consistent treatment of dust heating and emission in a three-dimensional radiative transfer code. Astrophys. J. **551**(1), 277–293 (2001). https://doi.org/10.1086/320083. arXiv:astro-ph/0011576 [astro-ph]

Mollá, M., Cavichia, O., Gavilán, M., et al.: Galactic chemical evolution: stellar yields and the initial mass function. Mon. Not. R. Astron. Soc. **451**(4), 3693–3708 (2015). https://doi.org/10.1093/mnras/stv1102. arXiv:1505.03341 [astro-ph.GA]

Moos, W.: The Lyman far ultraviolet spectroscopic explorer. Adv. Space Res. **11**(11), 221–227 (1991). https://doi.org/10.1016/0273-1177(91)90079-Y

Morales-Calderón, M., Stauffer, J.R., Hillenbrand, L.A., et al.: Ysovar: the first sensitive, wide-area, mid-infrared photometric monitoring of the orion nebula cluster. Astrophys. J. **733**(1), 50 (2011). https://doi.org/10.1088/0004-637X/733/1/50. arXiv:1103.5238 [astro-ph.SR]

Mordasini, C., Alibert, Y., Benz, W.: Extrasolar planet population synthesis. I. Method, formation tracks, and mass-distance distribution. Astron. Astrophys. **501**(3), 1139–1160 (2009a). https://doi.org/10.1051/0004-6361/200810301. arXiv:0904.2524 [astro-ph.EP]

Mordasini, C., Alibert, Y., Benz, W., et al.: Extrasolar planet population synthesis. II. Statistical comparison with observations. As-

tron. Astrophys. **501**(3), 1161–1184 (2009b). https://doi.org/10.1051/0004-6361/200810697. arXiv:0904.2542 [astro-ph.EP]

Moura, T., Alencar, S.H.P., Sousa, A.P., et al.: Spectroscopic analysis of accretion/ejection signatures in the Herbig Ae/Be stars HD 261941 and V590 Mon. Mon. Not. R. Astron. Soc. **494**(3), 3512–3535 (2020). https://doi.org/10.1093/mnras/staa695

Muijres, L.E., de Koter, A., Vink, J.S., et al.: Predictions of the effect of clumping on the wind properties of O-type stars. Astron. Astrophys. **526**, A32 (2011). https://doi.org/10.1051/0004-6361/201014290

Mullan, D.J.: Corotating interaction regions in stellar winds. Astrophys. J. **283**, 303–312 (1984). https://doi.org/10.1086/162307.

Najita, J.R., Strom, S.E., Muzerolle, J.: Demographics of transition objects. Mon. Not. R. Astron. Soc. **378**(1), 369–378 (2007). https://doi.org/10.1111/j.1365-2966.2007.11793.x. arXiv:0704.1681 [astro-ph]

Neiner, C.: The UVMag space project: UV and visible spectropolarimetry of massive stars. In: Meynet, G., Georgy, C., Groh, J., et al. (eds.) New Windows on Massive Stars, pp. 389–390 (2015). https://doi.org/10.1017/S1743921314007212. 1407.8082

Nikzad, S., Hoenk, M.E., Grunthaner, P.J., et al.: Delta-doped CCDs: high QE with long-term stability at UV and visible wavelengths. In: Crawford, D.L., Craine, E.R. (eds.) Instrumentation in Astronomy VIII, pp. 907–915 (1994). https://doi.org/10.1117/12.176733

Nikzad, S., Jewell, A.D., Hoenk, M.E., et al.: High-efficiency UV/optical/NIR detectors for large aperture telescopes and UV explorer missions: development of and field observations with delta-doped arrays. J. Astron. Telesc. Instrum. Syst. **3**, 036002 (2017). https://doi.org/10.1117/1.JATIS.3.3.036002. arXiv:1612.04734 [astro-ph.IM]

Nikzad, S., Hamden, E., Hoenk, M., et al.: Special section guest editorial: detectors for astronomy and cosmology. J. Astron. Telesc. Instrum. Syst. **6**, 011001 (2020). https://doi.org/10.1117/1.JATIS.6.1.011001

Nordsieck, K.H., Code, A.D., Anderson, C.M., et al.: Exploring ultraviolet astronomical polarimetry: results from the Wisconsin Ultraviolet Photo-Polarimeter Experiment (WUPPE). In: Fineschi, S. (ed.) X-Ray and Ultraviolet Polarimetry, pp. 2–11 (1994). https://doi.org/10.1117/12.168568

Nugis, T., Crowther, P.A., Willis Astron, J.: Clumping-corrected mass-loss rates of Wolf-Rayet stars. Astron. Astrophys. **333**, 956–969 (1998)

Oksala, M.E., Kochukhov, O., Krtička, J., et al.: Revisiting the rigidly rotating magnetosphere model for σ Ori E – II. Magnetic Doppler imaging, arbitrary field RRM, and light variability. Mon. Not. R. Astron. Soc. **451**(2), 2015–2029 (2015). https://doi.org/10.1093/mnras/stv1086. arXiv:1505.04839 [astro-ph.SR]

Owocki, S.P., Castor, J.I., Rybicki, G.B.: Time-dependent models of radiatively driven stellar winds. I. Nonlinear evolution of instabilities for a pure absorption model. Astrophys. J. **335**, 914 (1988). https://doi.org/10.1086/166977

Owocki, S.P., ud-Doula, A., Sundqvist, J.O., et al.: An 'analytic dynamical magnetosphere' formalism for X-ray and optical emission from slowly rotating magnetic massive stars. Mon. Not. R. Astron. Soc. **462**(4), 3830–3844 (2016). https://doi.org/10.1093/mnras/stw1894. arXiv:1607.08568 [astro-ph.SR]

Panopoulou, G.V., Tassis, K., Skalidis, R., et al.: Demonstration of magnetic field tomography with starlight polarization toward a diffuse sightline of the ISM. Astrophys. J. **872**(1), 56 (2019). https://doi.org/10.3847/1538-4357/aafdb2. arXiv:1809.09804 [astro-ph.GA]

Péroux, C., Howk, J.C.: The cosmic baryon and metal cycles. Annu. Rev. Astron. Astrophys. **58**, 363–406 (2020). https://doi.org/10.1146/annurev-astro-021820-120014. arXiv:2011.01935 [astro-ph.GA]

Perraut, K., Dougados, C., Lima, G.H.R.A., et al.: A disk wind in AB Aurigae traced with Hα interferometry. Astron. Astrophys. **596**, A17 (2016). https://doi.org/10.1051/0004-6361/201628931

Pertenais, M., Neiner, C., Parès, L., et al.: Preliminary design of the full-Stokes UV and visible spectropolarimeter for UVMag/Arago. In: Nagendra, K.N., Bagnulo, S., Centeno, R., et al.(eds.): Polarimetry pp. 168–174 (2015). https://doi.org/10.1017/S1743921315004718. 1502.00856

Peters, G., Gayley, K., Ignace, R., et al.: Ultraviolet Spectropolarimetry: Conservative and Nonconservative Mass Transfer in OB Interacting Binaries. Astrophys. Space Sci. **367** (2022). https://doi.org/10.1007/s10509-022-04106-w

Petit, V., Owocki, S.P., Wade, G.A., et al.: A magnetic confinement versus rotation classification of massive-star magnetospheres. Mon. Not. R. Astron. Soc. **429**(1), 398–422 (2013). https://doi.org/10.1093/mnras/sts344. arXiv:1211.0282 [astro-ph.SR]

Petit, V., Keszthelyi, Z., MacInnis, R., et al.: Magnetic massive stars as progenitors of 'heavy' stellar-mass black holes. Mon. Not. R. Astron. Soc. **466**(1), 1052–1060 (2017). https://doi.org/10.1093/mnras/stw3126. arXiv:1611.08964 [astro-ph.SR]

Petrenz, P., Puls, J.: 2-D non-LTE models of radiation driven winds from rotating early-type stars. I. Winds with an optically thin continuum. Astron. Astrophys. **358**, 956–992 (2000)

Praderie, F., Simon, T., Catala, C., et al.: Short-term spectral variability in AB Aurigae: clues for activity in Herbig AE stars. I. The ultraviolet lines of MG II and Fe II. Astrophys. J. **303**, 311 (1986). https://doi.org/10.1086/164076

Prinja, R.K., Massa, D.L.: Signature of wide-spread clumping in B supergiant winds. Astron. Astrophys. **521**, L55 (2010). https://doi.org/10.1051/0004-6361/201015252. arXiv:1007.2744 [astro-ph.SR]

Puls, J., Vink, J.S., Najarro, F.: Mass loss from hot massive stars. Astron. Astrophys. Rev. **16**(3–4), 209–325 (2008). https://doi.org/10.1007/s00159-008-0015-8. arXiv:0811.0487 [astro-ph]

Purcell, E.M.: Suprathermal rotation of interstellar grains. Astrophys. J. **231**, 404–416 (1979). https://doi.org/10.1086/157204

Quijada, M.A., Del Hoyo, J., Rice, S.: Enhanced far-ultraviolet reflectance of MgF_2 and LiF over-coated Al mirrors. In: Takahashi, T., den Herder, J.W.A., Bautz, M. (eds.) Space Telescopes and Instrumentation 2014: Ultraviolet to Gamma Ray, p. 91444G (2014). https://doi.org/10.1117/12.2057438

Quijada, M.A., del Hoyo, J., Boris, D.R., et al.: Improved mirror coatings for use in the Lyman ultraviolet to enhance astronomical instrument capabilities. In: Society of Photo-Optical Instrumentation Engineers (SPIE) Conference Series, p. 103980Z (2017). https://doi.org/10.1117/12.2274790

Rebull, L.M., Cody, A.M., Covey, K.R., et al.: Young Stellar Object VARiability (YSOVAR): long timescale variations in the mid-infrared. Astron. J. **148**(5), 92 (2014). https://doi.org/10.1088/0004-6256/148/5/92. arXiv:1408.6756 [astro-ph.SR]

Rich, E.A., Wisniewski, J.P., Currie, T., et al.: Multi-epoch direct imaging and time-variable scattered light morphology of the HD 163296 protoplanetary disk. Astrophys. J. **875**(1), 38 (2019). https://doi.org/10.3847/1538-4357/ab0f3b. arXiv:1811.07785 [astro-ph.SR]

Richardson, L.L., Brown, J.C., Simmons, J.F.L.: Polarimetric versus photometric variability and the density of WR star wind inhomogeneities. Astron. Astrophys. **306**, 519 (1996)

Rodrigues, C.V., Magalhães, A.M.: Blobs in wolf-rayet winds: random photometric and polarimetric variability. Astrophys. J. **540**(1), 412–421 (2000). https://doi.org/10.1086/309291. arXiv:astro-ph/0003362 [astro-ph]

Rodriguez, J.E., Ansdell, M., Oelkers, R.J., et al.: Identification of Young stellar variables with KELT for K2. I. Taurus dippers and rotators. Astrophys. J. **848**(2), 97 (2017). https://doi.org/10.3847/1538-4357/aa8c78. arXiv:1703.02522 [astro-ph.SR]

Russell, S.C., Dopita, M.A.: Abundances of the heavy elements in the magellanic clouds. III. Interpretation of results. Astrophys. J. **384**, 508 (1992). https://doi.org/10.1086/170893

Sana, H., de Koter, A., de Mink, S.E., et al.: The VLT-FLAMES Tarantula survey. VIII. Multiplicity properties of the O-type star population. Astron. Astrophys. **550**, A107 (2013). https://doi.org/10.1051/0004-6361/201219621. arXiv:1209.4638 [astro-ph.SR]

Sander, A.A.C., Vink, J.S., Hamann, W.R.: Driving classical Wolf-Rayet winds: a Γ- and Z-dependent mass-loss. Mon. Not. R. Astron. Soc. **491**(3), 4406–4425 (2020). https://doi.org/10.1093/mnras/stz3064. arXiv:1910.12886 [astro-ph.SR]

Sanders, J.T.: Comparison of measured and analytical ultraviolet light attenuation. In: Straka, S.A., Carosso, N. (eds.) Optical System Contamination: Effects, Measurements, and Control 2010. International Society for Optics and Photonics, vol. 7794, pp. 204–208. SPIE, Bellingham (2010). https://doi.org/10.1117/12.862165

Schaerer, D., de Koter, A.: Combined stellar structure and atmosphere models for massive stars. III. Spectral evolution and revised ionizing fluxes of O3-B0 stars. Astron. Astrophys. **322**, 598–614 (1997). arXiv:astro-ph/9611068 [astro-ph]

Schulte-Ladbeck, R.E., Shepherd, D.S., Nordsieck, K.H., et al.: Evidence for a bipolar nebula around the peculiar B[e] star HD 45677 from ultraviolet spectropolarimetry. Astrophys. J. **401**, L105 (1992). https://doi.org/10.1086/186682

Scowen, P.A., Tripp, T., Beasley, M., et al.: Finding the UV-Visible Path Forward: Proceedings of the Community Workshop to Plan the Future of UV/Visible Space Astrophysics, vol. 076, p. 001 (2017). https://doi.org/10.1088/1538-3873/129/977/076001. arXiv:1611.09736 [astro-ph.IM]

Shultz, M., Wade, G.A.: Confirming the oblique rotator model for the extremely slowly rotating O8f?p star HD 108. Mon. Not. R. Astron. Soc. **468**(4), 3985–3992 (2017). https://doi.org/10.1093/mnras/stx759. arXiv:1703.08996 [astro-ph.SR]

Shultz, M.E., Wade, G.A., Rivinius, T., et al.: The magnetic early B-type stars – III. A main-sequence magnetic, rotational, and magnetospheric biography. Mon. Not. R. Astron. Soc. **490**(1), 274–295 (2019). https://doi.org/10.1093/mnras/stz2551. arXiv:1909.02530 [astro-ph.SR]

Shultz, M.E., Owocki, S., Rivinius, T., et al.: The magnetic early B-type stars – IV. Breakout or leakage? H α emission as a diagnostic of plasma transport in centrifugal magnetospheres. Mon. Not. R. Astron. Soc. **499**(4), 5379–5395 (2020). https://doi.org/10.1093/mnras/staa3102. arXiv:2009.12336 [astro-ph.SR]

Shultz, M.E., Rivinius, T., Wade, G.A., et al.: MOBSTER – V. Discovery of a magnetic companion star to the magnetic β Cep pulsator HD 156424. Mon. Not. R. Astron. Soc. **504**(4), 4850–4864 (2021). https://doi.org/10.1093/mnras/staa3158. arXiv:2010.04221 [astro-ph.SR]

Shultz, M.E., Casini, R., Cheung, M.C.M., et al.: Ultraviolet Spectropolarimetry with Polstar: Using Polstar to test Magnetospheric Mass-loss Quenching. Astrophys. Space Sci. **367** (2022) https://doi.org/10.1007/s10509-022-04113-x

Sikora, J., Wade, G.A., Power, J., et al.: A volume-limited survey of mCP stars within 100 pc II: rotational and magnetic properties. Mon. Not. R. Astron. Soc. **483**(3), 3127–3145 (2019). https://doi.org/10.1093/mnras/sty2895. arXiv:1811.05635 [astro-ph.SR]

Sitko, M.L., Carpenter, W.J., Kimes, R.L., et al.: Variability of disk emission in pre-main-sequence and related stars. I. HD 31648 and HD 163296: isolated Herbig Ae stars driving herbig-haro flows. Astrophys. J. **678**(2), 1070–1087 (2008). https://doi.org/10.1086/529003. arXiv:0712.4014 [astro-ph]

Smartt, S.J.: Observational constraints on the progenitors of core-collapse supernovae: the case for missing high-mass stars. Publ. Astron. Soc. Aust. **32**, e016 (2015). https://doi.org/10.1017/pasa.2015.17. arXiv:1504.02635 [astro-ph.SR]

Snik, F., van Harten, G., Navarro, R., et al.: Design of a full-Stokes polarimeter for VLT/X-shooter. In: McLean, I.S., Ramsay, S.K., Takami, H. (eds.) Ground-Based and Airborne Instrumentation for Astronomy IV, p. 844625 (2012). https://doi.org/10.1117/12.926163. 1207.2965

St.-Louis, N., Willis Astron, J., Stevens, I.R.: Ultraviolet observations of selective wind eclipses in gamma velorum and evidence for colliding winds. Astrophys. J. **415**, 298 (1993). https://doi.org/10.1086/173165

St-Louis, N., Tremblay, P., Ignace, R.: Polarization light curve modelling of corotating interaction regions in the wind of the Wolf-Rayet star WR 6. Mon. Not. R. Astron. Soc. **474**(2), 1886–1899 (2018). https://doi.org/10.1093/mnras/stx2813. arXiv:1710.09724 [astro-ph.SR]

St-Louis, N., Gayley, K., Hillier, D., et al.: UV Spectropolarimetry with Polstar: Massive Star Binary Colliding Winds. Astrophys. Space Sci. **367** (2022) https://doi.org/10.1007/s10509-022-04102-0

Stenflo, J.: Solar Magnetic Fields: Polarized Radiation Diagnostics, vol. 189 (1994). https://doi.org/10.1007/978-94-015-8246-9

Stenflo, J.O.: The hanle effect and the diagnostics of turbulent magnetic fields in the solar atmosphere. Sol. Phys. **80**(2), 209–226 (1982). https://doi.org/10.1007/BF00147969

Sundqvist, J.O., Owocki, S.P., Puls, J.: 2D wind clumping in hot, massive stars from hydrodynamical line-driven instability simulations using a pseudo-planar approach. Astron. Astrophys. **611**, A17 (2018). https://doi.org/10.1051/0004-6361/201731718. arXiv:1710.07780 [astro-ph.SR]

Tannirkulam, A., Monnier, J.D., Millan-Gabet, R., et al.: Strong near-infrared emission interior to the dust sublimation radius of Young stellar objects MWC 275 and AB Aurigae. Astrophys. J. **677**(1), L51 (2008). https://doi.org/10.1086/587873. arXiv:0803.1484 [astro-ph]

Thaller, M.L., Bagnuolo JWilliam, G., Gies, D.R., et al.: Tomographic separation of composite spectra. III. Ultraviolet detection of the hot companion of phi persei. Astrophys. J. **448**, 878 (1995). https://doi.org/10.1086/176016

Tomczyk, S., Casini, R., de Wijn, A.G., et al.: Wavelength-diverse polarization modulators for Stokes polarimetry. Appl. Opt. **49**(18), 3580 (2010). https://doi.org/10.1364/AO.49.003580. arXiv:1006.3581 [astro-ph.IM]

Townsend, R.H.D., Owocki, S.P.: A rigidly rotating magnetosphere model for circumstellar emission from magnetic OB stars. Mon. Not. R. Astron. Soc. **357**(1), 251–264 (2005). https://doi.org/10.1111/j.1365-2966.2005.08642.x. arXiv:astro-ph/0408565 [astro-ph]

ud-Doula, A., Owocki, S.P.: Dynamical simulations of magnetically channeled line-driven stellar winds. I. Isothermal, nonrotating, radially driven flow. Astrophys. J. **576**(1), 413–428 (2002). https://doi.org/10.1086/341543. arXiv:astro-ph/0201195 [astro-ph]

Ud-Doula, A., Owocki, S.P., Townsend, R.H.D.: Dynamical simulations of magnetically channelled line-driven stellar winds – II. The effects of field-aligned rotation. Mon. Not. R. Astron. Soc. **385**(1), 97–108 (2008). https://doi.org/10.1111/j.1365-2966.2008.12840.x. arXiv:0712.2780 [astro-ph]

Ud-Doula, A., Owocki, S.P., Townsend, R.H.D.: Dynamical simulations of magnetically channelled line-driven stellar winds – III. Angular momentum loss and rotational spin-down. Mon. Not. R. Astron. Soc. **392**(3), 1022–1033 (2009). https://doi.org/10.1111/j.1365-2966.2008.14134.x. arXiv:0810.4247 [astro-ph]

van Bezooijen, R.W.H.: SIRTF autonomous star tracker. In: Mather, J.C. (ed.) IR Space Telescopes and Instruments, pp. 108–121 (2003). https://doi.org/10.1117/12.461606

Varga, J., Hogerheijde, M., van Boekel, R., et al.: The asymmetric inner disk of the Herbig Ae star HD 163296 in the eyes of VLTI/MATISSE: evidence for a vortex? Astron. Astrophys. **647**, A56 (2021). https://doi.org/10.1051/0004-6361/202039400. arXiv:2012.05697 [astro-ph.SR]

Vink, J.S., Drew, J.E., Harries, T.J., et al.: Resolved polarization changes across Hα in the classical T Tauri star RY Tauri. Astron.

Astrophys. **406**, 703–707 (2003). https://doi.org/10.1051/0004-6361:20030833. arXiv:astro-ph/0306095 [astro-ph]

Wade, G.A., Donati, J.F., Landstreet, J.D., et al.: High-precision magnetic field measurements of Ap and Bp stars. Mon. Not. R. Astron. Soc. **313**(4), 851–867 (2000). https://doi.org/10.1046/j.1365-8711.2000.03271.x

Waters, L.B.F.M., Waelkens, C.: Herbig Ae/Be stars. Annu. Rev. Astron. Astrophys. **36**, 233–266 (1998). https://doi.org/10.1146/annurev.astro.36.1.233

Whitney, B.A., Wood, K., Bjorkman, J.E., et al.: Two-dimensional radiative transfer in protostellar envelopes. II. An evolutionary sequence. Astrophys. J. **598**(2), 1079–1099 (2003a). https://doi.org/10.1086/379068. arXiv:astro-ph/0309007 [astro-ph]

Whitney, B.A., Wood, K., Bjorkman, J.E., et al.: Two-dimensional radiative transfer in protostellar envelopes. I. Effects of geometry on class I sources. Astrophys. J. **591**(2), 1049–1063 (2003b). https://doi.org/10.1086/375415. arXiv:astro-ph/0303479 [astro-ph]

Whitney, B.A., Indebetouw, R., Bjorkman, J.E., et al.: Two-dimensional radiative transfer in protostellar envelopes. III. Effects of stellar temperature. Astrophys. J. **617**(2), 1177–1190 (2004). https://doi.org/10.1086/425608

Whitney, B.A., Robitaille, T.P., Bjorkman, J.E., et al.: Three-dimensional radiation transfer in young stellar objects. Astrophys. J. Suppl. **207**(2), 30 (2013). https://doi.org/10.1088/0067-0049/207/2/30. arXiv:1307.0561 [astro-ph.SR]

Whittet, D.: (2003). Dust in the galactic environment

Wichittanakom, C., Oudmaijer, R.D., Fairlamb, J.R., et al.: The accretion rates and mechanisms of Herbig Ae/Be stars. Mon. Not. R. Astron. Soc. **493**(1), 234–249 (2020). https://doi.org/10.1093/mnras/staa169. arXiv:2001.05971 [astro-ph.SR]

Wisniewski, J., Berdyugin, A., Berdyugina, S., et al.: UV Spectropolarimetry with Polstar: Protoplanetary Disks. Astrophys. Space Sci. **367** (2022). https://doi.org/10.1007/s10509-022-04125-7

Wisniewski, J.P., Clampin, M., Grady, C.A., et al.: The HD 163296 circumstellar disk in scattered light: evidence of time-variable self-shadowing. Astrophys. J. **682**(1), 548–558 (2008). https://doi.org/10.1086/589629. arXiv:0807.1766 [astro-ph]

Wolff, M.J., Clayton, G.C., Kim, S.H., et al.: Ultraviolet interstellar linear polarization. III. Features. Astrophys. J. **478**(1), 395–402 (1997). https://doi.org/10.1086/303789

Wong, M.H., Baggett, S.M., Deustua, S., et al.: Overview of the WFC3 Cycle 17 Detector Monitoring Campaign. Instrument Science Report WFC3 2009-07, (2009). 8 pages

Yan, H., Lazarian, A.: Polarization of absorption lines as a diagnostics of circumstellar, interstellar, and intergalactic magnetic fields: fine-structure atoms. Astrophys. J. **653**(2), 1292–1313 (2006). https://doi.org/10.1086/508704. arXiv:astro-ph/0611281 [astro-ph]

Yan, H., Lazarian, A.: Atomic alignment and diagnostics of magnetic fields in diffuse media. Astrophys. J. **677**(2), 1401–1424 (2008). https://doi.org/10.1086/533410. arXiv:0711.0926 [astro-ph]

Yan, H., Lazarian, A.: Tracing magnetic fields with ground state alignment. J. Quant. Spectrosc. Radiat. Transf. **113**(12), 1409–1428 (2012). https://doi.org/10.1016/j.jqsrt.2012.03.027. arXiv:1203.5571 [astro-ph.GA]

Zhang, H., Gangi, M., Leone, F., et al.: Discovery of ground-state absorption line polarization and sub-Gauss magnetic field in the post-AGB binary system 89 her. Astrophys. J. **902**(1), L7 (2020). https://doi.org/10.3847/2041-8213/abb8e1. arXiv:1903.08675 [astro-ph.GA]

Zhu, Z.: Inclined massive planets in a protoplanetary disc: gap opening, disc breaking, and observational signatures. Mon. Not. R. Astron. Soc. **483**(3), 4221–4241 (2019). https://doi.org/10.1093/mnras/sty3358. arXiv:1812.01262 [astro-ph.EP]